

Generative model for learning quantum ensemble via optimal transport loss

Hiroyuki Tezuka^{*,1,2,3}, Shumpei Uno^{*,2,4}, and Naoki Yamamoto^{†,2,5}

¹Sony Group Corporation, 1-7-1 Konan, Minato-ku, Tokyo, 108-0075, Japan

²Quantum Computing Center, Keio University, Hiyoshi 3-14-1, Kohoku-ku, Yokohama 223-8522, Japan

³Graduate School of Science and Technology, Keio University, 3-14-1 Hiyoshi, Kohoku-ku, Yokohama, Kanagawa, 223-8522, Japan

⁴Mizuho Research & Technologies, Ltd., 2-3 Kanda-Nishikicho, Chiyoda-ku, Tokyo, 101-8443, Japan

⁵Department of Applied Physics and Physico-Informatics, Keio University, Hiyoshi 3-14-1, Kohoku-ku, Yokohama 223-8522, Japan

Abstract

Generative modeling is an unsupervised machine learning framework, that exhibits strong performance in various machine learning tasks. Recently we find several quantum version of generative model, some of which are even proven to have quantum advantage. However, those methods are not directly applicable to construct a generative model for learning a set of quantum states, i.e., ensemble. In this paper, we propose a quantum generative model that can learn quantum ensemble, in an unsupervised machine learning framework. The key idea is to introduce a new loss function calculated based on optimal transport loss, which have been widely used in classical machine learning due to its several good properties; e.g., no need to ensure the common support of two ensembles. We then give in-depth analysis on this measure, such as the scaling property of the approximation error. We also demonstrate the generative modeling with the application to quantum anomaly detection problem, that cannot be handled via existing methods. The proposed model paves the way for a wide application such as the health check of quantum devices and efficient initialization of quantum computation.

1 Introduction

In the recent great progress of quantum algorithms for both noisy near-term and future fault-tolerant quantum devices, particularly the quantum machine learning (QML) attracts huge attention. QML is largely categorised into two regimes in view of the type of data, which can be roughly called classical data and quantum data. The former has a conventional meaning used in the classical case; for the supervised learning scenario, e.g., a quantum system is trained to give a prediction for a given classical data such as an image. As for the latter, on the other hand, the task is to predict some property for a given quantum state drawn from a set of states, e.g., the phase of a many-body quantum state, again in the supervised learning scenario. Thanks to the obvious difficulty to directly represent a huge quantum state classically, some quantum advantage have been proven in QML for quantum data [1–3].

In the above paragraph we used the supervised learning setting to explain the difference of classical and quantum data. But the success of unsupervised learning in classical machine learning, particularly the generative modeling, is of course notable; actually a variety of algorithms have demonstrated strong performance in several applications, such as image generation [4–6], molecular design [7], and anomaly detection [8]. Hence, it is quite reasonable that several quantum unsupervised learning algorithms have been actively developed, such as quantum circuit born machine (QCBM) [9, 10], quantum generative adversarial network (QGAN) [11, 12], and quantum autoencoder (QAE) [13, 14]. Also, Ref. [12] studied the generative modeling problem for quantum data; the task is to construct a model quantum system producing a set of quantum states, i.e., *quantum ensemble*, that approximates a given quantum ensemble. The model quantum system contains latent variables, the change of which corresponds to the change of output quantum state of the system. In classical case, such generative model governed by latent variables is called an implicit model. It is known that, to efficiently train an implicit model, we are often encouraged to take the policy to minimize a distance between the model dataset and training dataset, rather than minimizing e.g., the divergence between two probability distributions. The *optimal transport loss (OTL)*, which typically leads to the Wasserstein distance, is suitable for the purpose of measuring the distance of two dataset; actually the quantum version of Wasserstein distance was proposed in [15, 16] and was applied to construct a generative model for quantum ensemble in QGAN framework [17, 18].

Along this line of research, in this paper we also focus on the generative modeling problem for quantum ensemble. We are motivated from the fact that the above-mentioned existing works employed the Wasserstein distance defined for two mixed quantum states corresponding to the training and model quantum ensembles, where each mixed state

*These authors equally contributed to this work.

†e-mail address: yamamoto@appi.keio.ac.jp

is obtained by compressing all element of the quantum ensemble to a single mixed state. This is clearly problematic, because this compression process loses a lot of information of the ensemble; for instance, single qubit pure states uniformly distributed on the equator of the Bloch sphere may be compressed to a maximally mixed state, which clearly does not recover the original ensemble. Accordingly, it is obvious that learning a single mixed state produced from the training ensemble does not lead to a model system that can approximate the original training ensemble.

In this paper, hence, we propose a new quantum OTL, which directly measures the difference between two quantum ensembles. The generative model can then be obtained by minimizing this quantum OTL between a training quantum ensemble and the ensemble of pure quantum states produced from the model. As the generative model, we use a parameterized quantum circuit (PQC) that contains tuning parameters and latent variables, which are both served by the angles of single-qubit rotation gates. A notable feature of the proposed OTL is that this has a form of sum of local functions that operates on a few neighboring qubits. This condition (i.e., the locality of the cost) is indeed necessary to train the model without suffering from the so-called vanishing gradient issue [19], meaning that the gradient vector with respect to the parameters decreases exponentially fast when increasing the number of qubits.

Using the proposed quantum OTL, which will be formally defined in Section 3, we will show the following result. The first result is given in Section 4, which provides performance analysis of OTL and its gradient from several aspects; e.g., scaling properties of OTL as a function of the number of training data and the number of measurement. We also numerically confirm that the gradient of OTL is certainly free from the vanishing gradient issue. The second result is provided in Section 5, showing some example of constructing a generative model for quantum ensemble by minimizing the OTL. This demonstration includes the application of quantum generative model to an anomaly detection problem of quantum data; that is, once a generative model is constructed by learning a given quantum ensemble, then it can be used to detect an anomaly quantum state by measuring the distance of this state to the output ensemble of the model. Section 6 gives a concluding remark, and some supporting materials including the proof of theorems are given in Appendix.

2 Preliminaries

In this section, we first review the implicit generative model for classical machine learning problems in Sec. 2.1. Next, Sec. 2.2 is devoted to describe the general OTL, which can be effectively used as a cost function to train a generative model.

2.1 Implicit Generative Model

The generative model is used to approximate an unknown probability distribution that produces a given training dataset. The basic strategy to construct a generative model is as follows; assuming the probability distribution $\alpha(\mathbf{x})$ behind the given training dataset $\{\mathbf{x}_i\}_{i=1}^M \in \mathcal{X}^M$, where \mathcal{X} denotes the space of random variables, we prepare a parameterized probability distribution $\beta_{\boldsymbol{\theta}}(\mathbf{x})$ and learn the parameters $\boldsymbol{\theta}$ that minimize an appropriate loss function defined on the training dataset.

In general, generative models are categorized to two types: *prescribed models* and *implicit models*. The prescribed generative modeling explicitly defines $\beta_{\boldsymbol{\theta}}(\mathbf{x})$ with the parameters $\boldsymbol{\theta}$. Then we can calculate the log-likelihood function of $\beta_{\boldsymbol{\theta}}(\mathbf{x}_i)$, and the parameters are determined by the maximum likelihood method, which corresponds to minimizing the Kullback-Leibler divergence $KL(\alpha||\beta_{\boldsymbol{\theta}})$. On the other hand, the implicit generative modeling does not give us an explicit form of $\beta_{\boldsymbol{\theta}}(\mathbf{x})$. An important feature of the implicit generative model is that it can easily describe a probability distribution whose random variables are confined on a hidden low-dimensional manifold; also the data-generation process can be interpreted as a physical process from a latent variable to the data [20]. Examples of the implicit generative model includes Variational Auto-Encoders [21], Generative Adversarial Networks [22], and the flow-based method [23]. This paper focuses on the implicit generative model.

In the implicit generative model we usually assume that the distribution behind the training data resides on a relatively low-dimensional manifold. That is, an implicit generative model is expressed as a map of a random latent variable \mathbf{z} onto \mathcal{X} ; \mathbf{z} resides in a latent space \mathcal{Z} whose dimension N_z is significantly smaller than that of the sample space, N_x . The latent random variable \mathbf{z} follows a known distribution $\gamma(\mathbf{z})$ such as a uniform distribution or a Gaussian distribution. That is, the implicit model distribution is given by $\beta_{\boldsymbol{\theta}} = G_{\boldsymbol{\theta}}\#\gamma$, where $\#$ is called the push-forward operator [24] which moves the distribution γ on \mathcal{Z} to a probability distribution on \mathcal{X} through the map $G_{\boldsymbol{\theta}}$. This implicit generative model is trained so that the set of samples generated from the model distribution are close to the set of training data, by adjusting the parameters $\boldsymbol{\theta}$ to minimize some appropriate cost function \mathcal{L} as follows:

$$\boldsymbol{\theta}^* = \arg \min_{\boldsymbol{\theta}} \mathcal{L}(\hat{\alpha}_M, \hat{\beta}_{\boldsymbol{\theta}, M_g}). \quad (2.1)$$

$\hat{\alpha}_M(\mathbf{x})$ and $\hat{\beta}_{\boldsymbol{\theta}, M_g} = G_{\boldsymbol{\theta}}\#\hat{\gamma}_{M_g}(\mathbf{z})$ denote empirical distributions defined with the sampled data $\{\mathbf{x}_i\}_{i=1}^M$ and $\{\mathbf{z}_i\}_{i=1}^{M_g}$, which follow the probability distributions $\alpha(\mathbf{x})$ and $\gamma(\mathbf{z})$, respectively:

$$\hat{\alpha}_M(\mathbf{x}) = \frac{1}{M} \sum_{i=1}^M \delta(\mathbf{x} - \mathbf{x}_i), \quad \hat{\gamma}_{M_g}(\mathbf{z}) = \frac{1}{M_g} \sum_{i=1}^{M_g} \delta(\mathbf{z} - \mathbf{z}_i). \quad (2.2)$$

2.2 Optimal Transport Loss

The OTL is used in various fields such as image analysis, natural language processing, and finance [24–27]. In particular, the OTL is widely used as a loss function in the generative modeling, mainly because it can be applicable even when the support of probability distributions do not match, and it can naturally incorporate the distance in the sample space \mathcal{X} [28–33]. The OTL is defined as the minimum cost of moving a probability distribution α to another distribution β :

Definition 1 (Optimal Transport Loss [34]).

$$\begin{aligned} \mathcal{L}_c(\alpha, \beta) &= \min_{\pi} \int c(\mathbf{x}, \mathbf{y}) d\pi(\mathbf{x}, \mathbf{y}), \\ \text{subject to } & \int \pi(\mathbf{x}, \mathbf{y}) d\mathbf{x} = \beta(\mathbf{y}), \quad \int \pi(\mathbf{x}, \mathbf{y}) d\mathbf{y} = \alpha(\mathbf{x}), \quad \pi(\mathbf{x}, \mathbf{y}) \geq 0, \end{aligned} \quad (2.3)$$

where $c(\mathbf{x}, \mathbf{y}) \geq 0$ is a non-negative function on $\mathcal{X} \times \mathcal{X}$ that represents the transport cost from \mathbf{x} to \mathbf{y} , and is called the ground cost. Also, we call the set of couplings π that minimizes $\mathcal{L}_c(\alpha, \beta)$ as the optimal transport plan.

In general, the OTL does not meet the axioms of metric between probability distributions; but it does when the ground cost is represented in terms of a metric function as follows:

Definition 2 (p-Wasserstein distance [35]). When the ground cost $c(\mathbf{x}, \mathbf{y})$ is expressed as $c(\mathbf{x}, \mathbf{y}) = d(\mathbf{x}, \mathbf{y})^p$ with a metric function $d(\mathbf{x}, \mathbf{y})$ and a real positive constant p , the p-Wasserstein distance is defined as

$$\mathcal{W}_p(\alpha, \beta) = \mathcal{L}_{d^p}(\alpha, \beta)^{1/p}. \quad (2.4)$$

The p-Wasserstein distance satisfies the conditions of metric between probability distributions. That is, for arbitrary probability distributions α, β, γ , the p-Wasserstein distance \mathcal{W}_p satisfies $\mathcal{W}_p(\alpha, \beta) \geq 0$ and $\mathcal{W}_p(\alpha, \beta) = \mathcal{W}_p(\beta, \alpha)$; also it satisfies $\mathcal{W}_p(\alpha, \beta) = 0 \Leftrightarrow \alpha = \beta$ and the triangle inequality $\mathcal{W}_p(\alpha, \gamma) \leq \mathcal{W}_p(\alpha, \beta) + \mathcal{W}_p(\beta, \gamma)$.

In general it is difficult to directly handle the probability distributions α and β_{θ} to minimize the OTL $\mathcal{L}_c(\alpha, \beta_{\theta})$. Instead, as mentioned in Eq. (2.1), we try to minimize the approximation of the OTL via the empirical distributions (2.2):

Definition 3 (Empirical estimator for optimal transport loss [35]).

$$\begin{aligned} \mathcal{L}_c(\hat{\alpha}_M, \hat{\beta}_{\theta, M_g}) &= \min_{\{\pi_{i,j}\}_{i,j=1}^{M, M_g}} \sum_{i=1}^M \sum_{j=1}^{M_g} c(\mathbf{x}_i, G_{\theta}(\mathbf{z}_j)) \pi_{i,j}, \\ \text{subject to } & \sum_{i=1}^M \pi_{i,j} = \frac{1}{M_g}, \quad \sum_{j=1}^{M_g} \pi_{i,j} = \frac{1}{M}, \quad \pi_{i,j} \geq 0. \end{aligned} \quad (2.5)$$

The empirical estimator converges as $\mathcal{L}_c(\hat{\alpha}_M, \hat{\beta}_{\theta, M_g}) \rightarrow \mathcal{L}_c(\alpha, \beta_{\theta})$ in the limit $M = M_g \rightarrow \infty$. In general, the speed of this convergence is of the order of $O(M^{-1/N_x})$ with N_x the dimension of the sample space \mathcal{X} [36], but the p-Wasserstein distance enjoys the following convergence law [37].

Theorem 4 (Convergence rate of p-Wasserstein distance). For the upper Wasserstein dimension $d_p^*(\alpha)$ (which is given in Definition 4 of [37]) of the probability distribution α , the following expression holds when s is larger than $d_p^*(\alpha)$:

$$\mathbb{E}[\mathcal{W}_p(\alpha, \hat{\alpha}_M)] \lesssim O(M^{-1/s}), \quad (2.6)$$

where the expectation \mathbb{E} is taken with respect to the samples drawn from the empirical distribution $\hat{\alpha}_M$.

Intuitively, the upper Wasserstein dimension $d_p^*(\alpha)$ can be interpreted as the support dimension of the probability distribution α , which corresponds to the dimension of the latent space, N_z , in the implicit generative model. Exploiting the metric properties of the p-Wasserstein distance, the following corollaries are immediately derived from Theorem 4:

Corollary 5 (Convergence rate of p-Wasserstein distance between empirical distributions sampled from a common distribution). Let $\hat{\alpha}_{1, M}$ and $\hat{\alpha}_{2, M}$ be two different empirical distributions sampled from a common distribution α . The number of samples is M in both empirical distributions. Then the following expression holds for $s > d_p^*(\alpha)$:

$$\mathbb{E}[\mathcal{W}_p(\hat{\alpha}_{1, M}, \hat{\alpha}_{2, M})] \lesssim O(M^{-1/s}), \quad (2.7)$$

where the expectation \mathbb{E} is taken with respect to the samples drawn from the empirical distributions $\hat{\alpha}_{1, M}$ and $\hat{\alpha}_{2, M}$.

Corollary 6 (Convergence rate of p-Wasserstein distance between different empirical distributions). Suppose that the upper Wasserstein dimension of the probability distributions α and β_{θ} is at most d_p^* , then the following expression holds for $s > d_p^*$:

$$\mathbb{E} \left[\left| \mathcal{W}_p(\alpha, \beta_{\theta}) - \mathcal{W}_p(\hat{\alpha}_M, \hat{\beta}_{\theta, M}) \right| \right] \lesssim O(M^{-1/s}), \quad (2.8)$$

where the expectation \mathbb{E} is taken with respect to the samples drawn from the empirical distribution $\hat{\alpha}_M$ and $\hat{\beta}_{\theta, M}$.

These corollaries indicate that the empirical estimator (2.5) is a good estimator if the intrinsic dimension of the training data and the dimension of the latent space N_z are sufficiently small, because the Wasserstein dimension d_p^* is almost the same as the intrinsic dimension of the training data and the latent dimension. In Sec. 4.1, we numerically see that similar convergence laws hold even when the OTL is not the p-Wasserstein distance.

3 Learning algorithm of generative model for quantum ensemble

In Sec. 3.1, we define the new quantum OTL that can be suitably used in the learning algorithm of the generative model for quantum ensemble. The learning algorithm is provided in Sec. 3.2.

3.1 Optimal transport loss with local ground cost

Our idea is to directly use Eq. (2.5) yet with the ground cost for quantum states, $c(|\psi\rangle, |\phi\rangle)$, rather than that for classical data vectors, $c(\mathbf{x}, \mathbf{y})$. This actually enables us to define the OTL between quantum ensembles $\{|\psi_i\rangle\}$ and $\{|\phi_i\rangle\}$, as follows:

$$\mathcal{L}_c(\{|\psi_i\rangle\}, \{|\phi_i\rangle\}) = \min_{\{\pi_{i,j}\}} \sum_{i,j} c(|\psi_i\rangle, |\phi_j\rangle) \pi_{i,j}, \text{ subject to } \sum_i \pi_{i,j} = q_j, \sum_j \pi_{i,j} = p_i, \pi_{i,j} \geq 0, \quad (3.1)$$

where p_i and q_j are probabilities that $|\psi_i\rangle$ and $|\phi_j\rangle$ appears, respectively. Note that we can define the transport loss between the corresponding mixed states $\sum_i p_i |\psi_i\rangle \langle \psi_i|$ and $\sum_j q_j |\phi_j\rangle \langle \phi_j|$ or some modification of them, as discussed in [17]; but as mentioned in Sec. 1, such mixed state loses the original configuration of ensemble (e.g., single qubit pure states uniformly distributed on the equator of the Bloch sphere) and thus are not applicable to our purpose.

Then our question is how to define the ground cost $c(|\psi\rangle, |\phi\rangle)$. An immediate choice might be the trace distance:

Definition 7 (Trace distance for pure states [38]).

$$c_{\text{tr}}(|\psi\rangle, |\phi\rangle) = \sqrt{1 - |\langle \psi | \phi \rangle|^2}. \quad (3.2)$$

Because the trace distance satisfies the axioms of metric, we can define the p-Wasserstein distance for quantum ensembles, $\mathcal{W}_p(\{|\psi_i\rangle\}, \{|\phi_i\rangle\}) = \mathcal{L}_{d^p}(\{|\psi_i\rangle\}, \{|\phi_i\rangle\})^{1/p}$, which allows us to have some useful properties described in Corollary 5. It is also notable that the trace distance is relatively easy to compute on a quantum computer, using e.g. the swap test [39] or the inversion test [40].

We now give an important remark. As will be formally described, our goal is to find a quantum circuit that produces a quantum ensemble (via changing latent variables) which best approximates a given quantum ensemble. This task can be executed by the gradient descent method for a parametrized quantum circuit, but a naive setting leads to the vanishing gradient issue, meaning that the gradient vector decays to zero exponentially fast with respect to the number of qubits [19]. There have been several proposals found in the literature [41, 42], but a common prerequisite is that the cost should be a *local* one. To explain the meaning, let us consider the case where $|\phi\rangle$ is given by $|\phi\rangle = U |0\rangle^{\otimes n}$ where U is a unitary matrix (which will be a parametrized unitary matrix $U(\boldsymbol{\theta})$ defining the generative model) and n is the number of qubits. Then the trace distance is based on the fidelity $|\langle \psi | \phi \rangle|^2 = |\langle \psi | U |0\rangle^{\otimes n}|^2$. This is the probability to get all zeros via the *global* measurement on the state $U^\dagger |\psi\rangle$ in the computational basis, which thus means that the trace distance is a global cost; accordingly, the fidelity-based learning method suffers from the vanishing gradient issue. On the other hand, we find that the following cost function is based on the localized fidelity measurement.

Definition 8 (Ground cost for quantum states only with local measurements [43, 44]).

$$c_{\text{local}}(|\psi\rangle, |\phi\rangle) = c_{\text{local}}(|\psi\rangle, U |0\rangle^{\otimes n}) = \sqrt{\frac{1}{n} \sum_{k=1}^n (1 - p^{(k)})}, \quad (3.3)$$

$$p^{(k)} = \text{Tr} [P_0^k U^\dagger |\psi\rangle \langle \psi| U], \quad P_0^k = \mathbb{I}_1 \otimes \mathbb{I}_2 \otimes \cdots \otimes \overbrace{|0\rangle \langle 0|}_k \otimes \cdots \otimes \mathbb{I}_n,$$

where n is the number of qubits. Also, \mathbb{I}_i and $|0\rangle \langle 0|_i$ denote the identity operator and the projection operator that act on the i -th qubit, respectively; thus $p^{(k)}$ represents the probability of getting 0 when observing the k -th qubit.

Equation (3.3) is certainly a local cost, and thus it may be used for realizing effective learning free from the vanishing gradient issue provided that some additional conditions (which will be described in Section 5) are satisfied. However, importantly, $c_{\text{local}}(|\psi\rangle, |\phi\rangle)$ is not a distance between the two quantum states, because it is not symmetric and it does not satisfy the triangle inequality, while the trace distance (3.2) satisfies the axiom of distance. Yet $c_{\text{local}}(|\psi\rangle, |\phi\rangle)$ is always non-negative and becomes zero only when $|\psi\rangle = |\phi\rangle$, meaning that $c_{\text{local}}(|\psi\rangle, |\phi\rangle)$ functions as a divergence. Then we can prove that, in general, the OTL defined with a divergence ground cost also functions as a divergence, as follows. The proof is given in Appendix A.

Proposition 9. *When the ground cost $c(\mathbf{x}, \mathbf{y})$ is a divergence satisfying*

$$\begin{aligned} c(\mathbf{x}, \mathbf{y}) &\geq 0, \\ c(\mathbf{x}, \mathbf{y}) &= 0 \text{ iff } \mathbf{x} = \mathbf{y}, \end{aligned} \quad (3.4)$$

then the OTL $\mathcal{L}_c(\alpha, \beta)$ with $c(\mathbf{x}, \mathbf{y})$ is also a divergence. That is, $\mathcal{L}_c(\alpha, \beta)$ satisfies the following properties for arbitrary probability distributions α and β :

$$\begin{aligned} \mathcal{L}_c(\alpha, \beta) &\geq 0, \\ \mathcal{L}_c(\alpha, \beta) &= 0 \text{ iff } \alpha = \beta. \end{aligned} \quad (3.5)$$

Therefore, the OTL $\mathcal{L}_c(\{|\psi_i\rangle\}, \{|\phi_i\rangle\})$ given in Eq. (3.1) with the local ground cost $c_{\text{local}}(|\psi\rangle, |\phi\rangle)$ given in Eq. (3.3) functions as a divergence. This means that $\mathcal{L}_c(\{|\psi_i\rangle\}, \{|\phi_i\rangle\})$ can be suitably used for evaluating the difference between a given quantum ensemble and the set of output states of the generative model. At the same time, recall that, for the purpose of avoiding the gradient vanishing issue, we had to give up using the fidelity measure and accordingly the distance property of the OTL. Hence we directly cannot use the desirable properties described in Theorem 4, Corollary 5, and Corollary 6; nonetheless, in Section 4, we will discuss if similar properties do hold even for the divergence measure.

3.2 Learning Algorithm

The goal of our task is to train an implicit generative model so that it outputs a quantum ensemble approximating a given ensemble $\{|\psi_i\rangle\}_{i=1}^M$; that is, our generative model contains tunable parameters and latent variables, as in the classical case described in Section 2.1. In this paper, we employ the following implicit generative model:

Definition 10 (Implicit generative model on a quantum circuit). *Using the initial state $|0\rangle^{\otimes n}$ and the parameterized quantum circuit $U(\mathbf{z}, \boldsymbol{\theta})$, the implicit generative model on a quantum circuit is defined as*

$$|\phi_{\boldsymbol{\theta}}(\mathbf{z})\rangle = U(\mathbf{z}, \boldsymbol{\theta}) |0\rangle^{\otimes n}. \quad (3.6)$$

Here $\boldsymbol{\theta}$ is the vector of tunable parameters and \mathbf{z} is the vector of latent variables that follow a known probability distribution; both $\boldsymbol{\theta}$ and \mathbf{z} are encoded in the rotation angles of rotation gates in $U(\mathbf{z}, \boldsymbol{\theta})$.

The similar circuit model is also found in meta-VQE [45], which uses physical parameters such as the distance of atomic nucleus instead of random latent variables \mathbf{z} . Also, the model proposed in [12] introduces the latent variables \mathbf{z} as the computational basis of an initial state in the form $|\phi_{\boldsymbol{\theta}}(\mathbf{z})\rangle = U(\boldsymbol{\theta}) |\mathbf{z}\rangle$; however, in this model, states with different latent variables are always orthogonal with each other, and thus the model cannot capture a small change of state in the Hilbert space via changing the latent variables. In contrast, the model (3.6) fulfills this purpose as long as the expressivity of the state with respect to \mathbf{z} is enough. In addition, our model is advantageous in that the analytical derivative is available by the parameter shift rule [46, 47] not only for the tunable parameters $\boldsymbol{\theta}$ but also for the latent variables \mathbf{z} . This feature will be effectively utilized in the anomaly detection problem in Sec. 5.

Next, as for the learning cost, we take the following empirical estimator of OTL, calculated from the training data $\{|\psi_i\rangle\}_{i=1}^M$ and the samples of latent variables $\{\mathbf{z}_j\}_{j=1}^{M_g}$:

$$\begin{aligned} \mathcal{L}_{\text{local}} \left(\{|\psi_i\rangle\}_{i=1}^M, \{|\phi_{\boldsymbol{\theta}}(\mathbf{z}_j)\rangle\}_{j=1}^{M_g} \right) &= \min_{\{\pi_{i,j}\}_{i,j=1}^{M, M_g}} \sum_{i=1}^M \sum_{j=1}^{M_g} c_{\text{local}, i, j} \pi_{i, j}, \\ \text{subject to } \sum_{i=1}^M \pi_{i, j} &= \frac{1}{M_g}, \quad \sum_{j=1}^{M_g} \pi_{i, j} = \frac{1}{M}, \quad \pi_{i, j} \geq 0. \end{aligned} \quad (3.7)$$

where $c_{\text{local}, i, j}$ is the ground cost given by

$$\begin{aligned} c_{\text{local}, i, j} &= \sqrt{\frac{1}{n} \sum_{k=1}^n (1 - p_{i, j}^{(k)})}, \\ p_{i, j}^{(k)} &= \text{Tr} [P_0^k U^\dagger(\mathbf{z}_j, \boldsymbol{\theta}) |\psi_i\rangle \langle \psi_i| U(\mathbf{z}_j, \boldsymbol{\theta})], \quad P_0^k = \mathbb{I}_1 \otimes \mathbb{I}_2 \otimes \cdots \otimes \overbrace{|0\rangle \langle 0|_k}^{\text{k-th bit}} \otimes \cdots \otimes \mathbb{I}_n. \end{aligned} \quad (3.8)$$

Note that in practice $c_{\text{local}, i, j}$ is estimated with the finite number of measurements (shots); we denote $\tilde{c}_{\text{local}, i, j}^{(N_s)}$ to be the estimator with N_s shots for the ideal one $c_{\text{local}, i, j}$, and in this case the OTL is denoted as $\mathcal{L}_{\tilde{c}_{\text{local}}^{(N_s)}}$.

Based on the OTL (3.7), the pseudo-code of proposed algorithm is shown in Algorithm 1. The total number of training quantum states $|\psi_i\rangle$ required for the parameter update is of the order $O(MM_gN_s)$ in step 3, and $O(\max(M, M_g)N_sN_p)$ in step 5, since the parameter shift rule [46, 47] is applicable.

Algorithm 1 Learning Algorithm with Quantum Optimal Transport Loss (3.7)

Input: Quantum circuit model $U(\mathbf{z}, \boldsymbol{\theta})$ with initial parameters $\boldsymbol{\theta}$, learning rate ε , ensemble $\{|\psi_i\rangle\}$

Output: A quantum circuit that outputs an ensemble approximating the input ensemble

- 1: **repeat**
 - 2: Generate latent variables $\{\mathbf{z}_j\}_{j=1}^{M_g}$ sampled from the latent distribution.
 - 3: Estimate the ground costs $\{\tilde{c}_{\text{local},i,j}^{(N_s)}\}_{i,j=1}^{M,M_g}$ from $\{|\psi_i\rangle\}_{i=1}^M$ and $\{U(\mathbf{z}_j, \boldsymbol{\theta})\}_{j=1}^{M_g}$ with N_s shots, using Eq. (3.3).
 - 4: Calculate the optimal transport plan $\pi_{i,j}$ by solving the linear programming (3.7).
 - 5: Calculate the gradients $\left\{\frac{\partial}{\partial\theta_k}\mathcal{L}_{c_{\text{local}}}\right\}_{k=1}^{N_p}$ from $\pi_{i,j}$ and $\left\{\frac{\partial}{\partial\theta_k}\tilde{c}_{\text{local},i,j}^{(N_s)}\right\}_{i,j,k=1}^{M,M_g,N_p}$ using the parameter shift rule.
 - 6: Update $\{\theta_k\}_{k=1}^{N_p}$ by using the gradients $\left\{\frac{\partial}{\partial\theta_k}\mathcal{L}_{c_{\text{local}}}\right\}_{k=1}^{N_p}$ with learning rate ε .
 - 7: **until** convergence
-

4 Performance analysis of the cost and its gradient

In this section, we analyze the performance of the proposed OTL (3.7) and its gradient vector. First, in Sec. 4.1, we numerically study the approximation error of the loss with the focus on its dependence on the intrinsic dimension of data and the number of qubits, to see if the similar results to Theorem 4 and Corollaries 5 and 6 would hold even despite that the OTL is now a divergence rather than distance. Then, in Sec. 4.2, we provide numerical and theoretical analyses on the approximation error as a function of the number of measurement (shots). Finally, in Sec. 4.3, we numerically show that the OTL certainly avoids the vanishing gradient issue; i.e., thanks to the locality of the cost, the its gradient does not decay exponentially fast. All the analysis in this section is focused on the property of cost at a certain point of learning process (say, at the initial time); the performance analysis on the training process will be discussed in the next section.

We employ the parameterized unitary matrix $U(\mathbf{z}, \boldsymbol{\theta})$ shown in Fig. 1 to construct the implicit generative model (3.6), which is similar to that given in Ref. [19] except that our model contains the latent variables \mathbf{z} . That is, the model is composed of the following N_L repeated unitaries (we call each unitary the ℓ -th layer):

$$U_{N_L, \boldsymbol{\xi}, \boldsymbol{\eta}}(\mathbf{z}, \boldsymbol{\theta}) = \prod_{\ell=1}^{N_L} W V_{\boldsymbol{\xi}_\ell, \boldsymbol{\eta}_\ell}(\mathbf{z}, \boldsymbol{\theta}_\ell), \quad (4.1)$$

where $\boldsymbol{\theta}_\ell = \{\theta_{\ell,j}\}_{j=1}^n$, $\boldsymbol{\xi}_\ell = \{\xi_{\ell,j}\}_{j=1}^n$, and $\boldsymbol{\eta}_\ell = \{\eta_{\ell,j}\}_{j=1}^n$ are n -dimensional parameter vectors in the ℓ -th layer. We summarize these vectors to $\boldsymbol{\theta} = \{\boldsymbol{\theta}_\ell\}_{\ell=1}^{N_L}$, $\boldsymbol{\xi} = \{\boldsymbol{\xi}_\ell\}_{\ell=1}^{N_L}$, and $\boldsymbol{\eta} = \{\boldsymbol{\eta}_\ell\}_{\ell=1}^{N_L}$. Here $\boldsymbol{\theta}$ are trainable parameters and \mathbf{z} are latent variables. W is a fixed entangling unitary gate composed of the ladder-structured controlled- Z gates; that is, W operates the two-qubit controlled- Z gate on all adjacent qubits;

$$W = \prod_{i=1}^{n-1} CZ_{i,i+1}, \quad (4.2)$$

where $CZ_{i,i+1}$ is the controlled- Z gate acting on the i -th and $(i+1)$ -th qubits. The operator $V_{\boldsymbol{\xi}_\ell, \boldsymbol{\eta}_\ell}(\mathbf{z}, \boldsymbol{\theta}_\ell)$ consists of the single-qubit rotation operators:

$$V_{\boldsymbol{\xi}_\ell, \boldsymbol{\eta}_\ell}(\mathbf{z}, \boldsymbol{\theta}_\ell) = \prod_{i=1}^n R_{\xi_{\ell,i}}(\theta_{\ell,i} z_{\eta_{\ell,i}}), \quad (4.3)$$

where $R_{\xi_{\ell,i}}(\theta_{\ell,i} z_{\eta_{\ell,i}})$ is the single-qubit Pauli rotation operator with angle $\theta_{\ell,i} z_{\eta_{\ell,i}}$ and direction $\xi_{\ell,i} \in \{X, Y, Z\}$ in the ℓ -th layer, such as $R_X(\theta_{\ell,3} z_5) = \exp(-i\theta_{\ell,3} z_5 \sigma_x)$. The component of the latent variables, $\eta_{\ell,i} \in \{0, 1, 2, \dots, N_z\}$, and $\xi_{\ell,i} \in \{X, Y, Z\}$ are randomly chosen at the beginning of learning and never changed during learning. Also, we have introduced a constant bias term $z_0 = 1$ so that the ansatz $|\phi_\theta(\mathbf{z})\rangle = U(\mathbf{z}, \boldsymbol{\theta})|0\rangle^{\otimes n}$ can take a variety of states (for instance, if $z_1, \dots, z_{N_z} \sim 0$ in the absence of the bias, then $|\phi_\theta(\mathbf{z})\rangle$ is limited to around $|0\rangle^{\otimes n}$). We used Qiskit [48] in all the simulation studies.

4.1 Approximation error as a function of the number of training data

We have seen in Sec. 2.2 that, for the p-Wasserstein distance, the convergence rate of its approximation error is of the order $\mathcal{O}(M^{-1/s})$ rather than $\mathcal{O}(M^{-1/N_x})$, where M is the number of training samples, N_x is the dimension of the sample space \mathcal{X} , and s can be interpreted as the intrinsic dimension of the data or the latent space dimension. This is desirable, because in general $s \ll N_x$. However, the OTL (3.7) is not a distance but a divergence. Hence it is not clear if it could theoretically enjoy a similar error scaling, but in this subsection we give a numerical evidence to positively support this conjecture.

We present the following two types of numerical simulations. The aim of the first one (**Experiment A**) is to see if our OTL would satisfy a similar property to Eq. (2.7), which describes the difference of two empirical distributions

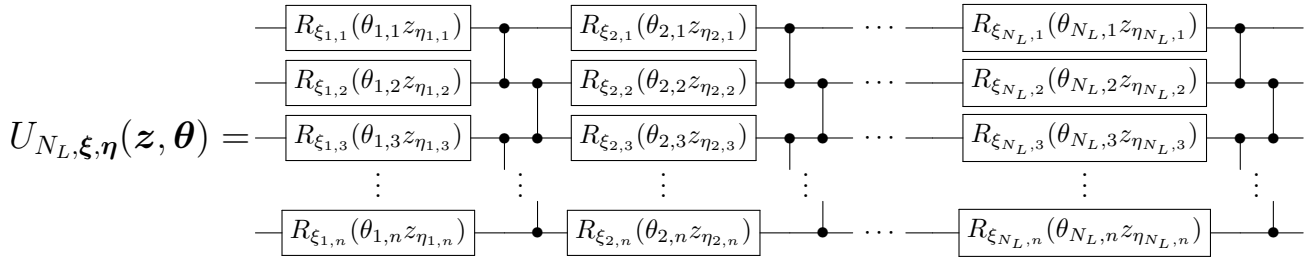


Figure 1: The structure of parameterized quantum circuit (ansatz) used in the performance analysis in Section 4 and sec:demonstration. This ansatz consists of the repeated layers with a similar structure. In the ℓ -th layer, the single qubit Pauli rotation operators with angles $\{\theta_{\ell,j} \times z_{\eta_{\ell,j}}\}_{j=1}^n$ and directions $\{\xi_{\ell,j}\}_{j=1}^n$ are applied to each qubit followed by a ladder-structured controlled-Z gate. The rotation angles $\xi = \{\xi_{\ell,j}\}_{\ell,j=1}^{N_L,n}$ and the components of the latent variables $\eta = \{\eta_{\ell,j}\}_{\ell,j=1}^{N_L,n}$ are randomly chosen at the beginning of the learning process and never changed during the learning.

Table 1: List of parameters for numerical simulation of Sec. 4.1

number of measurements	N_s	∞ (statevector)
number of training data	M	$\{2^i i \in \{0, 1, 2, \dots, 10\}\}$
number of Monte Carlo samples	N_{Monte}	100
number of qubits	n	$\{1, 2, 4, 6, 8, 10\}$ for Experiment A $\{1, 2, 4, 6, 8\}$ for Experiment B
dimension of latent space	N_z	$\{1, 2, 4, 6, 8\}$ for Experiment A $\{1, 2, 4, 6, 10, 14\}$ for Experiment B
number of layers	N_L	$3 + \lfloor N_z/n \rfloor$

sampled from the common hidden distribution. The second one (**Experiment B**) is studied for the case of Eq. (2.8), which describes the difference of the ideal OTL assuming the infinite samples available and an empirical distributions sampled from the common the ideal one. We used the statevector simulator [48] to calculate the OTL assuming the infinite number of measurement; in the next subsection, we will study the influence of the finite number of shots on the performance. Throughout all the numerical experiments, we randomly chose the parameters $\xi, \eta, \theta, \tilde{\xi}, \tilde{\eta}, \tilde{\theta}$ and did not change these values.

Experiment A. As an analogous quantity appearing in Eq. (2.7), we here focus on the following expected value of the empirical OTL defined in Eq. (3.7):

$$\mathbb{E}_{\tilde{z}, z \sim U(0,1)^{N_z}} \left[J_{\xi, \eta; \xi, \eta}^{\text{clocal}}(\tilde{z}, \tilde{\theta} : z, \theta; M) \right], \quad (4.4)$$

where

$$J_{\xi, \tilde{\eta}; \xi, \eta}^{\text{clocal}}(\tilde{z}, \tilde{\theta} : z, \theta; M) = \mathcal{L}_{\text{clocal}} \left(\{U_{N_L, \tilde{\xi}, \tilde{\eta}}(\tilde{z}_i, \tilde{\theta}) | 0\rangle^{\otimes n}\}_{i=1}^M, \{U_{N_L, \xi, \eta}(z_j, \theta) | 0\rangle^{\otimes n}\}_{j=1}^M \right). \quad (4.5)$$

In Eq. (4.4), we set $\xi = \tilde{\xi}$ and $\eta = \tilde{\eta}$ for the two unitary operators that appear in the argument of $\mathcal{L}_{\text{clocal}}$ in Eq. (4.5). This indicates that $J_{\xi, \eta; \xi, \eta}^{\text{clocal}}(\tilde{z}, \tilde{\theta} : z, \theta; M)$ in Eq. (4.4) would become zero in the limit of infinite number of training data ($M \rightarrow \infty$). The expectation in Eq. (4.4) is taken with respect to the latent variables \tilde{z}_i and z_j subjected to the N_z -dimensional uniform distribution $U(0, 1)^{N_z}$, but we numerically approximate it by N_{Monte} Monte Carlo samplings. Other conditions in the numerical simulation are shown in Table 1.

Figure 2 plots the values of Eq. (4.4) with several N_z (the dimension of the latent variables) and n (the number of qubits). In the figures, the dotted lines show the scaling curve M^{-1/N_z} . Notably, in the range of a large number of training data, the points and dotted lines are almost consistent, regardless of the number of qubits. This implies that the OTL for two different ensembles given by Eq. (4.4) is almost independent of the number of qubits n and depends mainly on the latent dimension N_z , likewise the case of distance-based loss function proven in Corollary 5.

Experiment B. We next turn to the second experiment to confirm that the approximation error of the proposed OTL scales similar to Eq. (2.8). Specifically, we numerically show the dependence of the following expectation value on the number of training data M :

$$\mathbb{E}_{\tilde{z}, z \sim U(0,1)^{N_z}} \left[\lim_{K \rightarrow \infty} J_{\xi, \tilde{\eta}; \xi, \eta}^{\text{clocal}}(\tilde{z}, \tilde{\theta} : z, \theta; K) - J_{\xi, \tilde{\eta}; \xi, \eta}^{\text{clocal}}(\tilde{z}, \tilde{\theta} : z, \theta; M) \right], \quad (4.6)$$

where J^{clocal} is defined in Eq. (4.5). In this case, we set different fixed parameters $\xi \neq \tilde{\xi}$ and $\eta \neq \tilde{\eta}$ for the two unitary operators in Eq. (4.5). The parameters used in the numerical simulation are shown in Table 1.

The first term of Eq. (4.6) is an ideal quantity assuming that an infinite number of training data is available. Since the first term is independent of the number of training data, the second term is expected to take the following form,

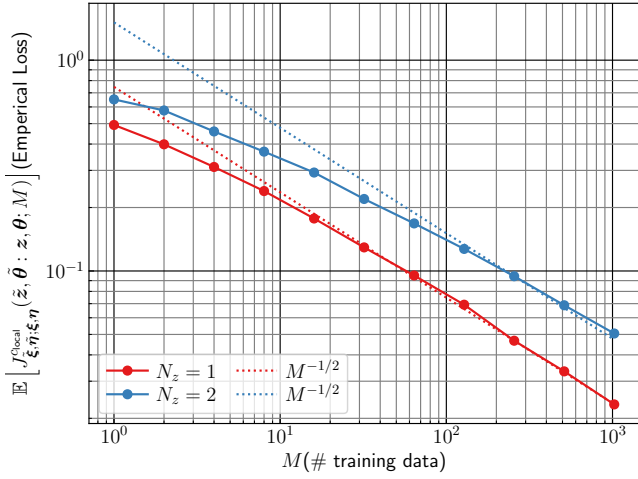
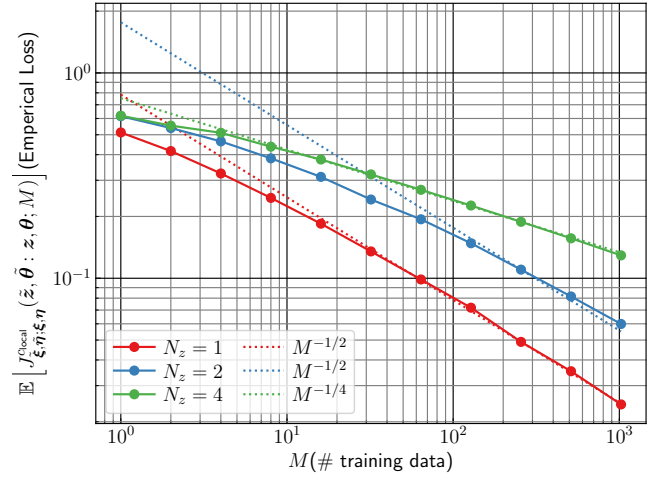
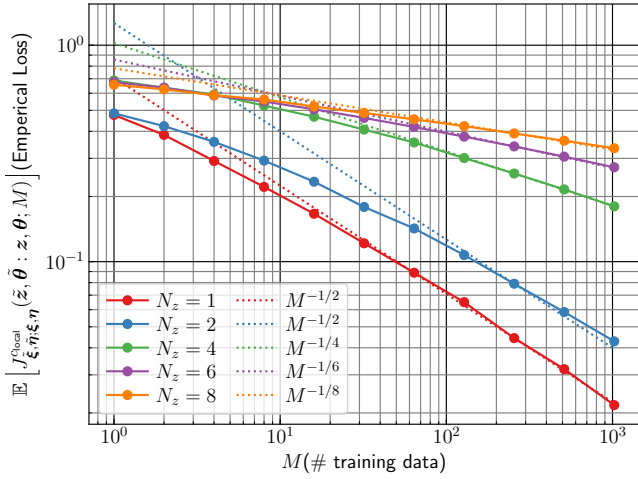
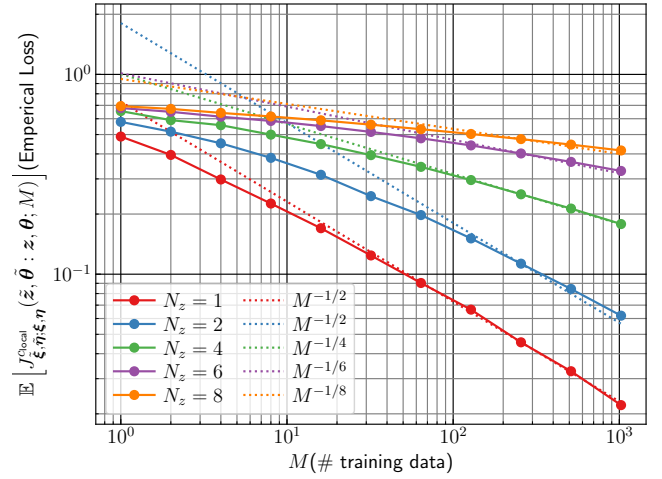
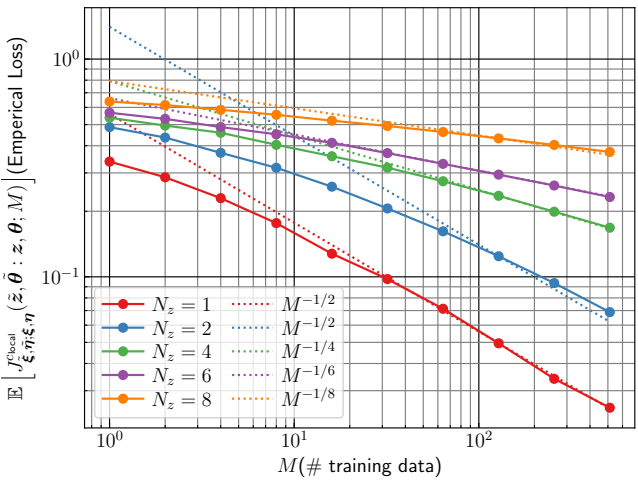
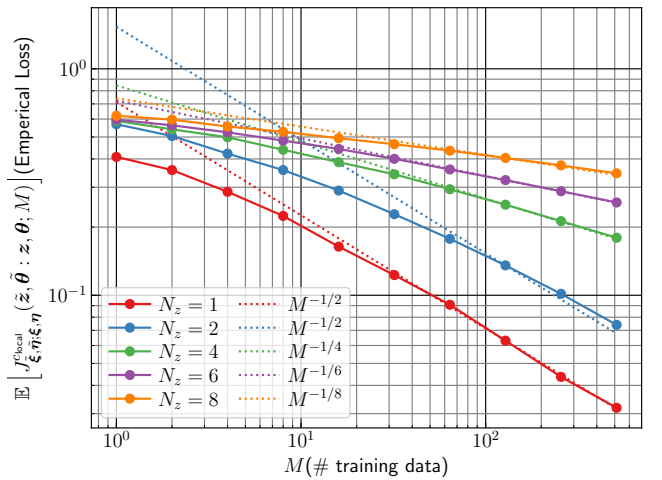
(a) $n = 1$ (b) $n = 2$ (c) $n = 4$ (d) $n = 6$ (e) $n = 8$ (f) $n = 10$

Figure 2: Results of numerical simulations on the relationship between the number of training data and the OTL given by Eq. (4.4), with several qubit number n . Each subgraph shows the results for various latent dimensions N_z . For reference, the scaling curves M^{-1/N_z} are added as dotted lines. These graphs show that Eq. (4.4) mainly scale as M^{-1/N_z} and are almost independent to the number of qubits, n .

as suggested from Eq. (2.8):

$$\mathbb{E}_{\tilde{\mathbf{z}}, \mathbf{z} \sim U(0,1)^{N_z}} \left[J_{\tilde{\xi}, \tilde{\eta}; \xi, \eta}^{\text{clocal}}(\tilde{\mathbf{z}}, \tilde{\boldsymbol{\theta}} : \mathbf{z}, \boldsymbol{\theta}; M) \right] = aM^{-1/b} + c. \quad (4.7)$$

To identify the parameter b , we use the Monte Carlo method to calculate the left hand side of Eq. (4.7) as a function of M and then execute the curve-fitting via $aM^{-1/b} + c$. We repeat this procedure with several values of the number of qubits n and the latent dimension N_z ; see Appendix B for a more detailed discussion. The result of parameter identification is depicted in Fig. 3, which shows that the fitting parameter b is almost independent to the number of qubits n and linearly scales with respect to the latent dimension N_z . This result is indeed consistent with Eq. (2.8).

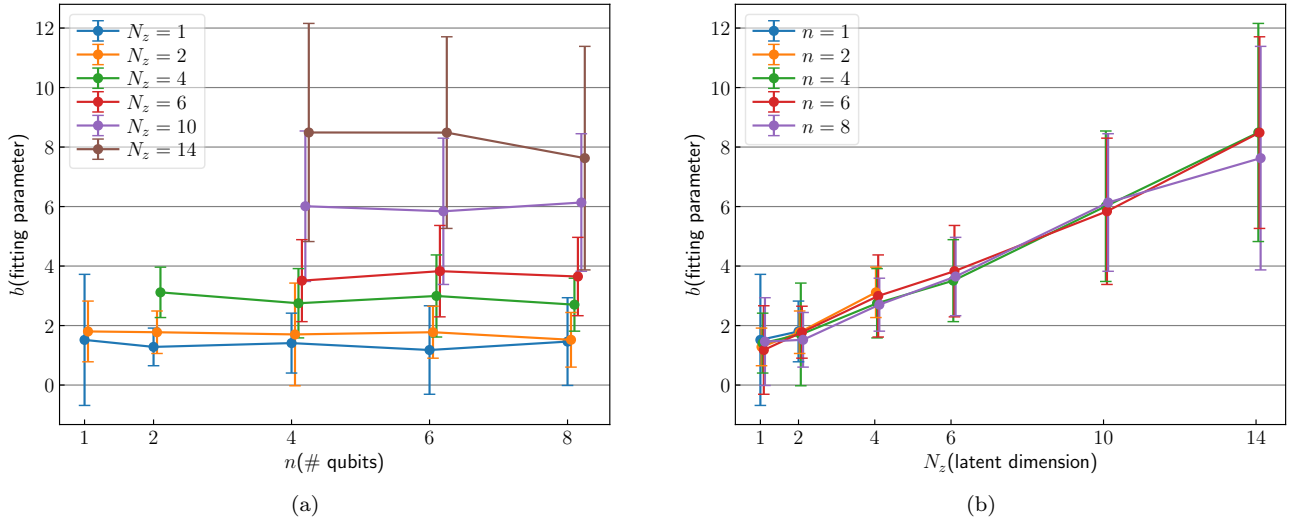


Figure 3: The simulation results of the fitting parameter b as a function of (a) the number of qubits n and (b) the latent dimension N_z . The fitting parameter b is obtained by fitting the second term of Eq. (4.6) by using Eq. (4.7). The subfigure (a) shows that b is almost independent to the number of qubits n , while the subgraph (b) shows that b linearly scales with the latent dimension N_z .

The results obtained in Experiments A and B suggest us to have the following conjecture:

Conjecture 11. *The scaling of the approximation error of the optimal transport loss (3.7) with respect to the number of training data M is determined via the latent dimension N_z as follows:*

$$\mathbb{E}_{\tilde{\mathbf{z}}, \mathbf{z} \sim U(0,1)^{N_z}} \left[\mathcal{L}_{\text{clocal}} \left(\{U(\tilde{\mathbf{z}}_i, \boldsymbol{\theta}) | 0\rangle^{\otimes n}\}_{i=1}^{\infty}, \{U(\mathbf{z}_j, \boldsymbol{\theta}) | 0\rangle^{\otimes n}\}_{j=1}^M \right) \right] \lesssim O(M^{-1/N_z}), \quad (4.8)$$

without respect to the number of qubits.

This conjecture means that the proposed OTL can be efficiently computed via sampling, when the intrinsic dimension of the data and the latent dimension are sufficiently small. Proving this conjecture would be challenging and is the subject of future work.

4.2 Approximation error as a function of the number of shots

The error analysis in Sec. 4.1 assumes that the number of shot is infinite and thereby the ground cost between quantum states can be perfectly determined. Here, we analyze the effect of the finiteness of the number of shots on the approximation error. The following proposition serves as a basis of the analysis.

Proposition 12. *Let $\tilde{c}_{\text{local}}^{(N_s)}$ be an estimator of the ground cost c_{local} of Eq. (3.3) using N_s samples. Suppose that the support of two different probability distributions are strictly separated; as a result, there exists a lower bound $g > 0$ to the ground cost for any $i, j \in \{1, 2, \dots, M\}$, i.e., $(c_{\text{local}}(|\psi_i\rangle, U(\mathbf{z}_j, \boldsymbol{\theta}) | 0\rangle^{\otimes n}) > g, \forall i, j)$. Then, for any positive constant δ , the following inequality holds:*

$$\begin{aligned} P \left(\left| \mathcal{L}_{\text{clocal}} \left(\{|\psi_i\rangle\}_{i=1}^M, \{U(\mathbf{z}_j, \boldsymbol{\theta}) | 0\rangle^{\otimes n}\}_{j=1}^M \right) - \tilde{c}_{\text{local}}^{(N_s)} \left(\{|\psi_i\rangle\}_{i=1}^M, \{U(\mathbf{z}_j, \boldsymbol{\theta}) | 0\rangle^{\otimes n}\}_{j=1}^M \right) \right| \right. \\ \left. \geq \sqrt{\frac{2M}{\delta}} \sqrt{\frac{1-g}{N_s} + \frac{(1-g)^2}{4N_s^2 g}} + \frac{1-g}{2N_s \sqrt{g}} \right) \leq \delta. \end{aligned} \quad (4.9)$$

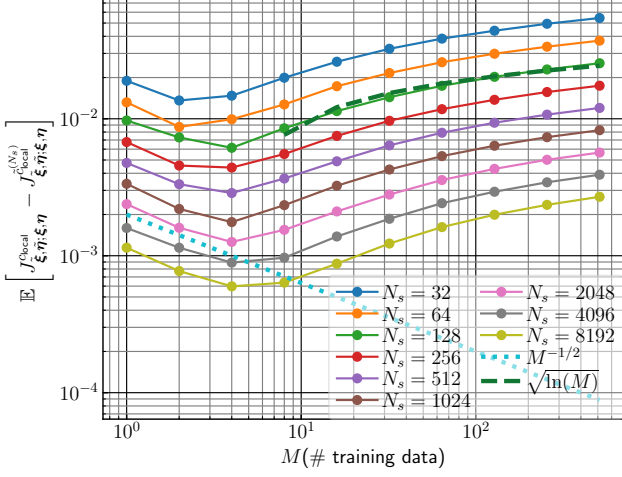
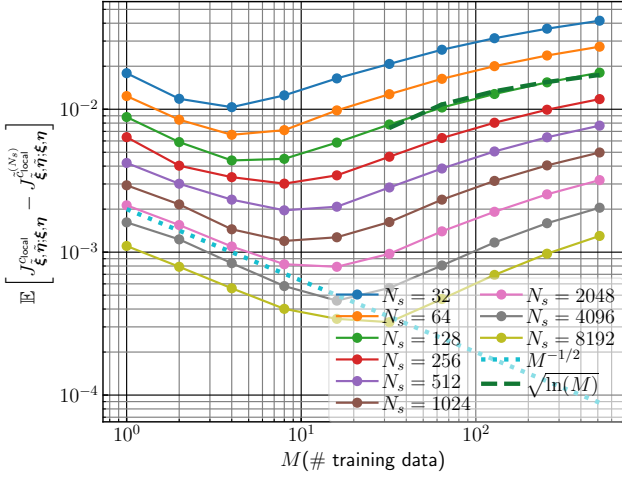
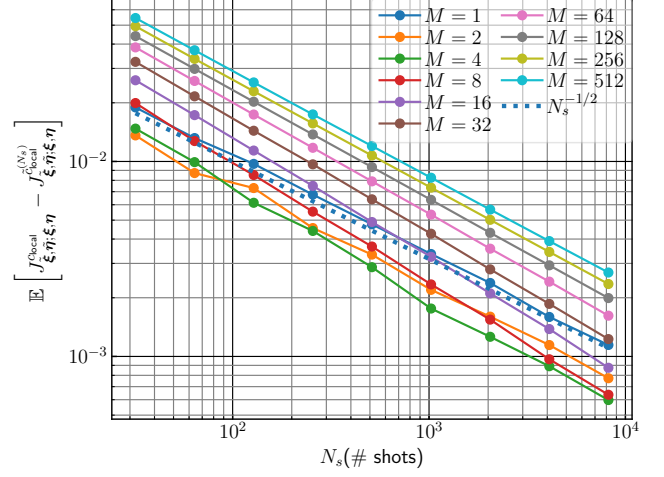
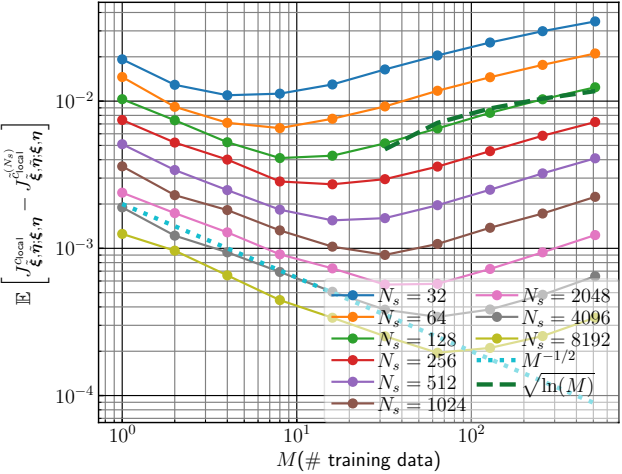
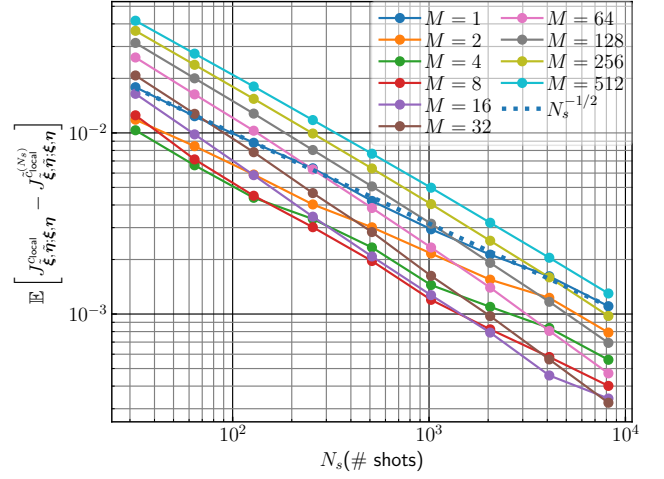
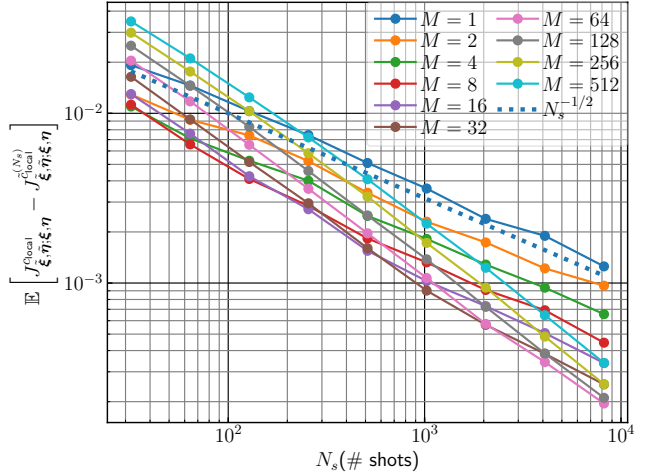
(a) $N_z = 1$ (b) $N_z = 2$ (c) $N_z = 4$ 

Figure 4: Simulation results of the approximation error of the OTL due to the number of shots defined in Eq. (4.10). The left and right panels show the dependence of the error on the number of training data M and shots N_s , respectively. The results for different latent dimension N_z are shown in the figures (a), (b), and (c). For reference, we added the curve of $M^{-1/2}$ with the dotted line in the left panels. The fitting result of the points $N_s = 128$ with the curve $\sqrt{c_1 \ln(M) + c_2}$ is added as the dashed line in the left panels. Also, we added the curve of $N_s^{-1/2}$ as the dotted line in the right panels.

Table 2: List of parameters for numerical simulation of Sec. 4.2

number of measurements	N_s	$\{2^{i+7} \mid i \in \{0, 1, 2, \dots, 7\}\}, \infty(\text{statevector})$
number of training data	M	$\{2^i \mid i \in \{0, 1, 2, \dots, 10\}\}$
number of Monte Carlo samples	N_{Monte}	256
number of qubits	n	8
dimension of latent space	N_z	$\{1, 2, 4\}$
number of layers	N_L	$3 + \lfloor N_z/n \rfloor$

The proof is shown in Appendix C. Proposition 12 states that the approximation error of the OTL is upper bounded by a constant of the order $O(\sqrt{M/N_s})$, under the condition $M \gg 1$ and $N_s \gg 1$. Therefore, if Observation 11 is true, the approximation error due to the finiteness of N_s and M is upper bounded by $O(M^{-1/N_z}) + O(\sqrt{M/N_s})$, where N_z is the latent dimension.

Then, we provide a numerical simulation to show the averaged approximation error as a function of M as well as N_s . Again, we employ the hardware efficient ansatz shown in Fig. 1 of Sec. 4.1. The purpose of the numerical simulation is to see the dependence of the following expectation value on M and N_s .

$$\mathbb{E}_{\tilde{\mathbf{z}}, \mathbf{z} \sim U(0,1)^{N_z}} \left[\left| J_{\tilde{\boldsymbol{\xi}}, \tilde{\boldsymbol{\eta}}; \boldsymbol{\xi}, \boldsymbol{\eta}}^{\tilde{\mathbf{z}}(N_z)}(\tilde{\mathbf{z}}, \tilde{\boldsymbol{\theta}}; \mathbf{z}, \boldsymbol{\theta}; M) - J_{\tilde{\boldsymbol{\xi}}, \tilde{\boldsymbol{\eta}}; \boldsymbol{\xi}, \boldsymbol{\eta}}^{\text{local}}(\tilde{\mathbf{z}}, \tilde{\boldsymbol{\theta}}; \mathbf{z}, \boldsymbol{\theta}; M) \right| \right], \quad (4.10)$$

where $J_{\tilde{\boldsymbol{\xi}}, \tilde{\boldsymbol{\eta}}; \boldsymbol{\xi}, \boldsymbol{\eta}}^{\tilde{\mathbf{z}}(N_z)}$ can be computed via Eq. (4.5). As in the numerical simulation in Sec. 4.1, we approximate the expectation $\mathbb{E}_{\tilde{\mathbf{z}}, \mathbf{z} \sim U(0,1)^{N_z}}[\bullet]$ by Monte Carlo sampling of $\tilde{\mathbf{z}}$ and \mathbf{z} from the uniform distribution $U(0,1)^{N_z}$. Also, we randomly choose the fixed parameters $\boldsymbol{\xi}, \boldsymbol{\eta}, \tilde{\boldsymbol{\xi}}, \tilde{\boldsymbol{\eta}}$ prior to the simulation. The other simulation parameters are given in Table 2. Simulation results are depicted in Fig. 4, where the notable points are summarized as follows.

- In the range of small number of training data M , the approximation error is roughly proportional to $M^{-1/2}$.
- In the range of large number of training data M , the approximation error takes $\sqrt{c_1 \ln M + c_2}$ with constants c_1 and c_2 .
- The dependence of the error on the number of shots N_s is roughly proportional to $N_s^{-1/2}$.

Appendix D provides an intuitive explanation of these results. In particular, it is important to know that we need to choose a proper number of samples to reduce the approximation error.

4.3 Avoidance of the vanishing gradient issue

In Sec. 3.1 we chose the cost function composed of the local measurements, as a least condition to avoid the vanishing gradient issue. Note that, however, employing a local cost is not enough to avoid this issue; for instance, Ref. [42] proposed the method of using a special type of parametrized quantum circuit called the *alternating layered ansatz* (ALA) in addition to using the local cost, which is actually proven to avoid the issue. Nevertheless, we here numerically demonstrate that our method can certainly mitigate the decrease of gradient even without such additional condition, compared to the case with global cost.

More specifically, we calculated the expectation of the variance of the partial derivative of the OTL (3.7), based on the training ensemble $\{|\psi_i\rangle\}_{i=1}^M$ and the sampled data from the generative model $\{U(\mathbf{z}_j, \boldsymbol{\theta})|0\rangle^{\otimes n}\}_{j=1}^M$;

$$\mathbb{V}_{\boldsymbol{\xi}, \boldsymbol{\eta}, \boldsymbol{\theta}, \mathbf{z}} \left[\frac{\partial}{\partial \boldsymbol{\theta}} \mathcal{L}_{\text{local}} \left(\{|\psi_i\rangle\}_{i=1}^M, \{U_{N_L, \boldsymbol{\xi}, \boldsymbol{\eta}}(\mathbf{z}_j, \boldsymbol{\theta})|0\rangle^{\otimes n}\}_{j=1}^M \right) \right]. \quad (4.11)$$

The partial derivative is calculated using the parameter shift rule [46]. The expectation of the variance is approximated by Monte Carlo calculations with respect to $\mathbf{z}, \boldsymbol{\xi}, \boldsymbol{\eta}$, and $\boldsymbol{\theta}$, where \mathbf{z} is sampled from the uniform distribution $U(0,1)$ and $\boldsymbol{\xi}, \boldsymbol{\eta}, \boldsymbol{\theta}$ are randomly chosen from $\boldsymbol{\xi} \in \{X, Y, Z\}^{nN_L}$, $\boldsymbol{\eta} \in \{0, 1, 2, \dots, N_z\}^{nN_L}$, and $\boldsymbol{\theta} \in [0, 2\pi]^{nN_L}$. The structure of the generative model $U(\mathbf{z}, \boldsymbol{\theta})|0\rangle^{\otimes n}$ is the same as that shown in Fig. 1. The derivative is taken with respect to $\theta_{1,1}$. The training ensemble $\{|\psi_i\rangle\}_{i=1}^M$ is prepared as follows;

$$|\psi\rangle_i = W' V_2'(\zeta_2^i) W' V_1'(\zeta_1^i) |0\rangle^{\otimes n},$$

where $\zeta_1^i = \{\zeta_{1,j}^i\}_{j=1}^n$ and $\zeta_2^i = \{\zeta_{2,j}^i\}_{j=1}^n$ are randomly chosen from the uniform distribution on $[0, 2\pi]$ and fixed during Monte Carlo calculation. The operators W', V_1' , and V_2' are defined as follows:

$$W' = \prod_{i=1}^{n-1} CX_{j,j+1}, \quad V_1'(\zeta_1^i) = \prod_{j=1}^n R_{j,Y}(\zeta_{1,j}^i), \quad V_2'(\zeta_2^i) = \prod_{j=1}^n R_{j,Z}(\zeta_{2,j}^i), \quad (4.12)$$

Table 3: List of parameters for numerical simulation of Sec. 4.3

number of measurements	N_s	∞ (statevector)
number of training data	M	$\{2^i \mid i \in \{1, 2, 3, 4\}\}$
number of Monte Carlo samples	N_{Monte}	300
number of qubits	n	$\{2, 4, 6, 8, 10, 12, 14\}$
dimension of latent space	N_z	$\{1\}$
number of layers	N_L	$\{10, 25, 50, 75, 100, 200\}$

where $CX_{j,k}$ denotes the controlled- X gate, which operates X gate on the k -th qubit with the j -th control qubit. $R_{j,Y}$ and $R_{j,Z}$ denote single qubit Pauli rotations around the x and y axes, respectively. The other simulation parameters are given in Table 3.

Figure 5 shows the numerical simulation result of the variance (4.11), for the cases where (a) the global cost (3.2) is used and (b) the local cost (3.3) is used. The number of training data is fixed to $M = 8$. The clear exponential decays in variance of gradient are observed for the global cost, regardless of N_L . In contrast, for the case of local cost, the relatively shallow circuits with $N_L = 10, 25$ exhibit approximately constant scaling with respect to $n \geq 10$, while the deep circuits with $N_L \geq 50$ also exhibit slower scaling than the global one and keep larger variance even when $n \geq 8$. This result implies that the OTL with local ground cost can avoid the gradient vanishing issue, despite that the circuit is not specifically designed for this purpose. Note also that the result is consistent with that reported in [49], which studied the cost function composed of single ground cost of our setting.

In addition, Fig. 5(c) shows the variance (4.11) as a function of the number of training data, M , in the case of $n = 14$. In the figure, the points represent the Monte-Carlo numerical results and the dotted lines represent the scaling curves M^{-x} where the value x is determined via fitting. This fitting result implies that the gradient obeys the simple statistical scaling with respect to M and thus the proposed algorithm would enjoy efficient learning even for a large training ensemble.

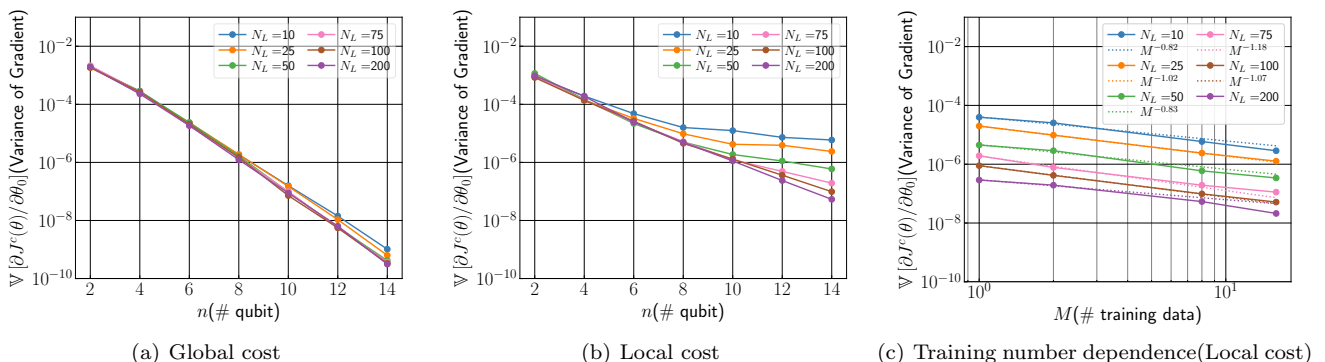


Figure 5: The gradient of the cost function as a function of the number of qubit, n , for the case of (a) the global cost (3.2) and (b) the local cost (3.3). Figure (c) shows the dependence on the number of training data, M , for the case of local cost. Several curves are depicted for different number of layers N_L . The clear exponential decay is observed in (a), but is avoided in (b). The polynomial decay ($\simeq M^{-1}$) is observed in (c), implying the simple statistical scaling.

5 Demonstration of the generative model training and application to anomaly detection

In this section, we present anomaly detection based on the cost function defined in Eq. (2.3) as a proof-of-concept of the proposed loss function.

5.1 Quantum Anomaly Detection

Anomaly detection is a task to judge whether a given test data $\mathbf{x}^{(t)}$ is anomalous (rare) data or not, based on the knowledge learned from the past training data $\mathbf{x}_i, (i = 1, 2, \dots, M)$, i.e., the generative model. Unlike typical classification tasks, this problem deals with a large imbalance in the number of normal data and that of anomalous data; actually, the former is usually much bigger than the latter. Therefore, typical classification methods are not suitable to solve this task, and some specialized schemes have been widely developed [50].

The anomaly detection problem is important in the field of quantum technology. That is, to realize accurate state preparation and control, we are required to detect contaminated quantum states and remove those states as quickly as possible. Previous quantum anomaly detection schemes rely on the measurement-based data processing [51, 52],

which however require a large number of measurement as in the case of quantum state tomography. In contrast, our anomaly detection scheme directly inputs quantum states to the constructed generative model and then diagnoses the anormality with much fewer measurements.

The following is the procedure for constructing the conventional anomaly detector based on the generative model [53], which we apply to our quantum case.

1. (*Distribution estimation*): Construct a model probability distribution from the normal dataset.
2. (*Anomaly score design*): Define an Anomaly Score (AS), based on the model distribution of normal data.
3. (*Threshold determination*): Set a threshold of AS for diagnosing the anormality.

Of these steps, the model probability distribution in Step 1 is constructed by the learning algorithm presented in Sec. 3.2. To designing the AS in Step 2, we refer to AnoGAN [54] in classical machine learning. Namely, we define a loss function $\mathcal{L}(U(\mathbf{z}, \boldsymbol{\theta}) |0\rangle^{\otimes n}, |\psi^{(t)}\rangle)$ for a test data $|\psi^{(t)}\rangle$ and the generative model $U(\mathbf{z}, \bar{\boldsymbol{\theta}})$ constructed from the training dataset with learned parameter $\bar{\boldsymbol{\theta}}$; then take the minimum with respect to the latent variables \mathbf{z} to calculate AS:

$$(\text{Anomaly Score}) = \min_{\mathbf{z}} \mathcal{L}(U(\mathbf{z}, \bar{\boldsymbol{\theta}}) |0\rangle^{\otimes n}, |\psi^{(t)}\rangle). \quad (5.1)$$

As the loss function \mathcal{L} , we use the local ground cost $c_{\text{local}}(|\psi^{(t)}\rangle, U(\mathbf{z}, \bar{\boldsymbol{\theta}}) |0\rangle^{\otimes n})$ defined in Eq. (3.3). The above minimization is executed via the gradient descent with respect to \mathbf{z} , which is obtained via the parameter shift rule similar to the derivative in θ . Algorithm 2 summarizes the procedure.

Algorithm 2 Algorithm to calculate Anomaly Score

Input: A trained quantum circuit $U(\mathbf{z}, \bar{\boldsymbol{\theta}})$, test data $\{|\psi^{(t)}\rangle\}$

Output: Anomaly Score

- 1: Initialize \mathbf{z}
 - 2: **repeat**
 - 3: Calculate the ground cost \mathcal{L} from $\{U(\mathbf{z}, \bar{\boldsymbol{\theta}})\}$ and $|\psi^{(t)}\rangle$ according to Eq. (3.3)
 - 4: Calculate the gradients $\left\{ \frac{\partial \mathcal{L}}{\partial z_k} \right\}_{k=1}^{N_z}$ using the parameter shift rule.
 - 5: Update \mathbf{z} by using the gradient descent method via $\left\{ \frac{\partial \mathcal{L}}{\partial z_k} \right\}_{k=1}^{N_z}$
 - 6: **until** convergence
-

5.2 Distributed dataset

The first demonstration is to construct a generative model that learns a quantum ensemble distributed on the equator of the generalized Bloch sphere. That is, the training ensemble (i.e., the normal dataset) $\{|\psi_j\rangle\}_{j=1}^M$ to be learned is set as follows:

$$|\psi_j\rangle = \cos(\pi/4) |0\rangle + e^{2\pi i \phi^j} \sin(\pi/4) |2^n - 1\rangle, \quad (5.2)$$

where ϕ^j is randomly generated from the uniform distribution on $[0, 1]$ and $|x\rangle$ denotes the x -th basis in the 2^n -dimensional Hilbert space. Note that the configuration of this ensemble cannot be learned by the existing mixed-state-based quantum anomaly detection scheme [51, 52], because the mixed state corresponding to this ensemble is nearly the maximally mixed state, the learning of which thus does not give us a generative model recovering the original ensemble.

We employ the same ansatz as that given in Sec. 4 with the parameters shown in Table 4 and construct the generative model according to Algorithm 1. As the optimizer, we take Adam [55] with learning rate 0.01. The number of learning iterations (i.e., the number of the updates of the parameters) is set to 1500 for $n = 2$ and 10000 for $n = 10$.

Once the model for normal ensemble is constructed, it is then used to anomaly detection. Here the set of test data $\{|\psi^{(t)}\rangle\}$ is given by

$$|\psi^{(t)}\rangle = \cos\left(\frac{\pi}{2}\theta^{(t)}\right) |0\rangle + e^{2\pi i \phi^{(t)}} \sin\left(\frac{\pi}{2}\theta^{(t)}\right) |2^n - 1\rangle, \quad (5.3)$$

where $\theta^{(t)}, \phi^{(t)} \in \{0, 0.1, 0.2, \dots, 2\}$. We calculate the AS using Algorithm 2. The other simulation parameters are shown in Table 4.

The numerical simulation result in the case of $n = 2, 10$ are presented in Figs. 6 and 7, respectively. The training ensemble is shown in the figure (a), where each blue point corresponds to the generalized Bloch vector. Some output states of the constructed generative model, corresponding to different value of $z \in [0, 1]$, are shown in the figure (b). Both of the red and blue points in Fig. (c) represent the test data state (5.3). The figure (d) shows the calculated AS, where the blue and red plots correspond to the blue and red points in (c), respectively. The dotted line in (d) illustrates the theoretical expected values assuming that the model completely learns the training data.

Table 4: List of parameters for numerical simulation in Sec. 5.2

number of measurements (training)	N_s	100 (for $n = 2$), ∞ (for $n = 10$)
number of measurements (anomaly detection)	N_{ad}	50 (for $n = 2$), 100 (for $n = 10$)
number of training data	M	30
number of qubits	n	2, 10
dimension of latent space	N_z	1
number of layers	N_L	10

Firstly, we see the clear correlation between the AS and the theoretical curve in Fig. 6, implying that AS is appropriately calculated via the proposed method. In the practical usecase, a user defines a threshold of AS depending on the task and then compare the calculated AS with the threshold for identifying the anomaly quantum states. For instance, if we set the threshold as $AS = 0.3$, the test states conditioned in $0.3 \leq \theta^{(t)}/\pi \leq 0.7$ in Fig. 6 are judged as normal while others are anomaly. Moreover, the output states of the learned generative model and the result of anomaly detection in the case of $n = 10$ are shown in Fig. 7. Although, the result displayed in (b) would suggest that the learning fails, the output states show correlation with the training states displayed in (a); actually, the output states live on the xy -plane in the generalized Bloch sphere spanned by $|0\rangle^{\otimes 10}$ and $|1\rangle^{\otimes 10}$. In addition, it is notable that only $N_s = 100$ is enough even for the case of $n = 10$ to perform anomaly detection, provided that we obtain an appropriate generative model from the training normal states. This is an advantage for practical situation, as this indicates that the proposed method may scale up with respect to the number of qubits.

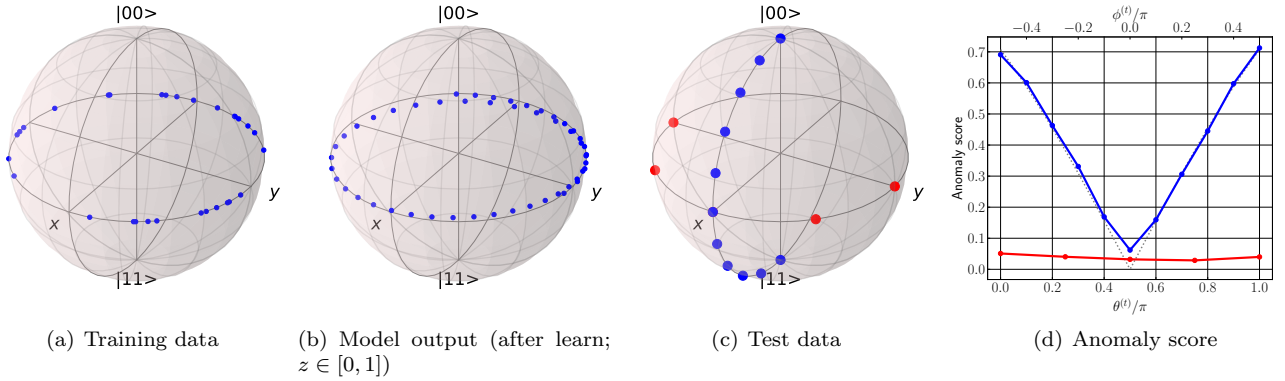


Figure 6: The simulation results in the case of $n = 2$, for the distributed training ensemble. (a) Generalized Bloch vector representation of training ensemble. (b) Output states from the generative model with latent variables $z \in [0, 1]$. (c) Test data (both red and blue points). (d) Anomaly scores for different test data. The blue and red plots correspond to the blue and red points in (c), respectively. The values of angle $\theta^{(t)}$ and $\phi^{(t)}$ are given in the bottom and upper horizontal axis, respectively. The dotted line represents the theoretical value of AS.

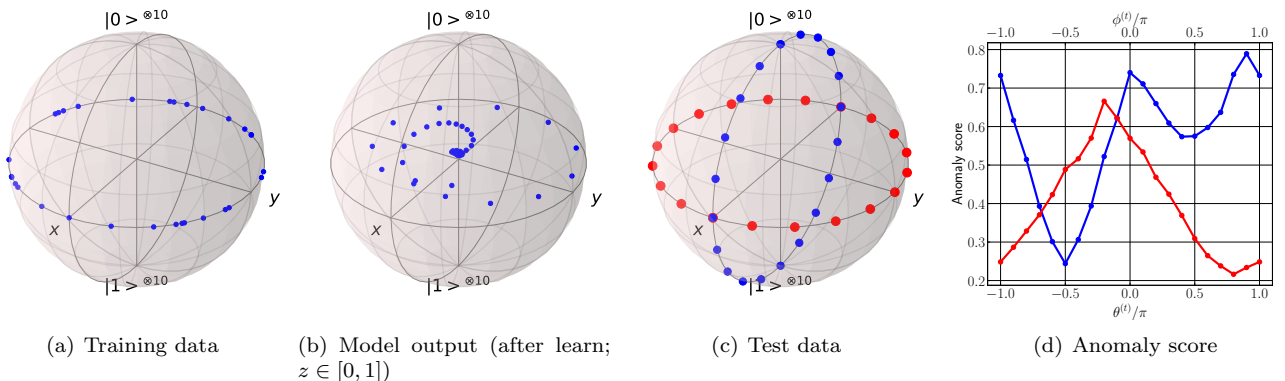


Figure 7: The simulation results in the case of $n = 10$, for the distributed training ensemble. (a) Generalized Bloch vector representation of training states. (b) Output states from the generative model with latent variables $z \in [0, 1]$. (c) Test data (both red and blue points). (d) Anomaly scores for different test data. The blue and red plots correspond to the blue and red points in (c), respectively. The values of angle $\theta^{(t)}$ and $\phi^{(t)}$ are given in the bottom and upper horizontal axis, respectively.

Table 5: List of parameters for numerical simulation of Sec. 5.3

number of measurements (training)	N_s	1000
number of measurements (anomaly detection)	N_{ad}	50
number of training data	M	10
number of qubits	n	6, 10
dimension of latent space	N_z	2
number of layers	N_L	10

5.3 Localized dataset

Next let us consider localized quantum ensemble. That is, the state of training ensemble $\{|\psi_j\rangle\}_{j=1}^M$ corresponding to the normal dataset is given by

$$|\psi_j\rangle = \cos\left(\frac{\pi}{2}\Delta\theta_j\right)|0\rangle + e^{2\pi i\Delta\phi_j}\sin\left(\frac{\pi}{2}\Delta\theta_j\right)|2^n - 1\rangle, \quad (5.4)$$

where n is the number of qubits. $\Delta\theta_j$ and $\Delta\phi_j$ are sampled from the normal distribution $N(\mu, \sigma)$ and the uniform distribution $U(a, b)$, respectively (μ and σ represent the mean and the variance, respectively). We will consider the two cases $(\mu, \sigma, a, b) = (0, 0.02, 0, 0.1)$ for $n = 6$ and $(\mu, \sigma, a, b) = (0, 0.02, 0, 0.2)$ for $n = 10$. Note that in this choice of parameters, the ensemble $\{|\psi_j\rangle\}_{j=1}^M$ is nearly two-dimensionally distributed on the generalized Bloch sphere, as illustrated in Fig. 9 (a, d). The other simulation parameters are shown in Table 5.

To construct a generative model via learning this two dimensional distribution, we set the dimension of latent variable as $N_z = 2$ from the above-mentioned observation on the dimensionality of $\{|\psi_j\rangle\}_{j=1}^M$. Also, we here take the so-called alternating layered ansatz (ALA), which, together with the use of local cost, is guaranteed to mitigate the gradient vanishing issue [41, 42]. This ansatz is more favorable than the previous one which we here call the hardware efficient ansatz (HEA), in view of the possibility to avoid the gradient vanishing issue. Therefore it is worth comparing their learning curves. Typical learning curves are shown in Fig. 8. The blue plots, which are labeled "local", represent the case where the cost is the local one (3.3) and the ansatz is ALA; thus we denote this case as L-ALA. On the other hand, the orange plots, which are labeled "global", represent the case where the cost is the global one (3.2) and the ansatz is HEA; thus we denote this case as G-HEA. Not that both displayed costs are calculated as the global one, to directly compare them; that is, the "local" represents the cost calculated at each iteration based on the global cost with the parameters that optimize the local cost. We observe that L-ALA has a clear advantage over G-HEA in terms of the convergence speed. This result coincides with that of Sec. 4.3, indicating the advantage of the local cost. In addition to the convergence speed, the final cost of L-ALA is lower than that of G-HEA. Note that the learning performance heavily depends on the initial random seed, yet it was indeed difficult to find a successful setting of G-HEA; actually in all cases we tried the trajectory seemed to be trapped in a local minima, presumably because the variance of G-HEA is much smaller than that of L-ALA.

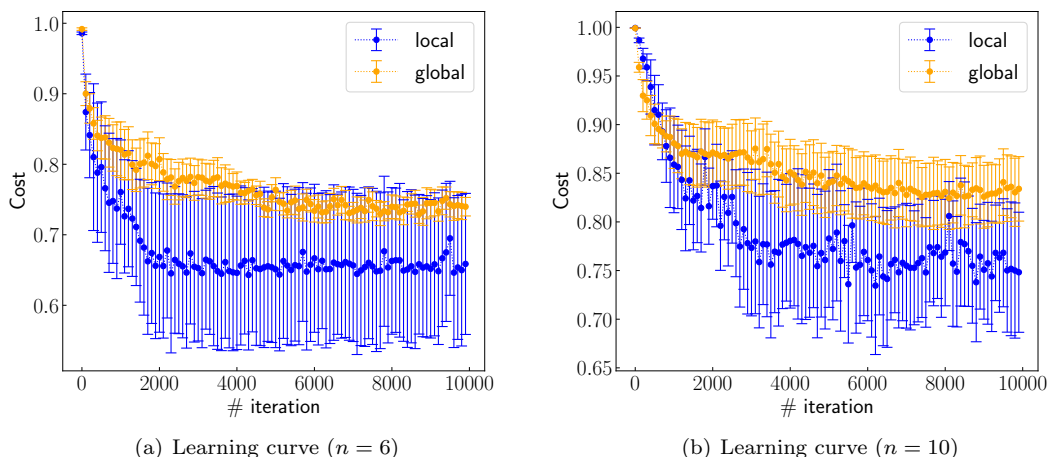


Figure 8: Learning curves for the case (a) $n = 6$ and (b) $n = 10$. The values of OTL is calculated with the parameters at each iteration trained with local cost (3.3) or global cost (3.2). Note that the displayed are the cost calculated with the global one (3.2) for both blue and orange cases, for fair comparison. The range of error bar is 1 standard deviation.

We apply the constructed generative model to the anomaly detection problem. In Fig. 9 (b) and (e), the test quantum states are displayed for the case of $n = 6$ and $n = 10$, respectively. The resultant anomaly score for each test

data are shown in Fig. 9 (c, f). In both cases, we can say that the models are trained appropriately. In particular, the variance of the distribution of $\{|\psi_j\rangle\}_{j=1}^M$, i.e., the distribution of the blue points in (a, d), is well captured by the width of the dip of red lines in (c, f). Finally note that, in this section, we use QASM simulator for the numerical simulation; the number of shot is 1000 for each measurement in the learning process, and 50 for the anomaly detection task, even for the case of $n = 10$. Compared to the state tomography, these numbers of shot are clearly too small. Nonetheless, the proposed method enabled the model to learn the training ensemble with such small number of shots.

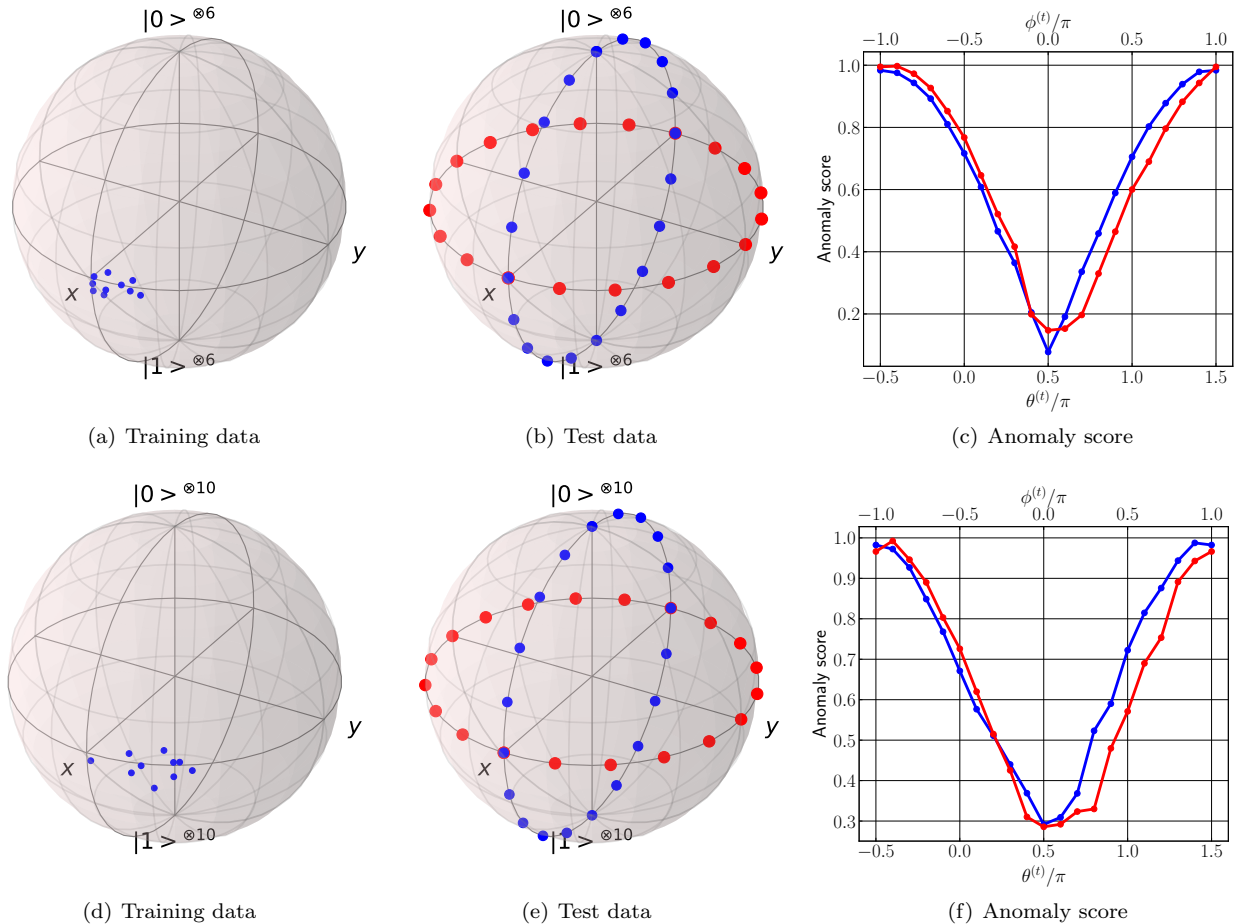


Figure 9: The simulation results for the localized training ensemble, in the case of (a,b,c) $n = 6$ and (d,e,f) $n = 10$. (a, d) Generalized Bloch vector representation of training states. (b, e) Test data (both red and blue points). (c, f) Anomaly scores for different test data. The blue and red plots correspond to the blue and red points in (b, e), respectively. The values of angle $\theta^{(t)}$ and $\phi^{(t)}$ are given in the bottom and upper horizontal axis, respectively. The dotted line represents the theoretical value of AS.

6 Conclusion

In classical machine learning, many generative models are vigorously studied, but there are only a few studies on quantum generative models for quantum data. This paper offers a new approach for building such a quantum generative model, i.e., learning method for quantum ensemble with unsupervised machine learning setting. For that purpose, we proposed a loss function based on optimal transport loss (OTL), which can be effectively used even when both the target and model probability distributions are hard to characterize. We also adopted the previously proposed local cost as the ground cost of OTL, to avoid the vanishing gradient problem and thereby increase learnability, but this makes OTL being no longer a distance. Hence we have shown that OTL with the local cost satisfies the properties of divergence between probability distributions and confirmed that the proposed OTL is suitable as a cost for generative model. We then theoretically and numerically analyzed the properties of the proposed OTL. Our analysis indicates that the proposed OTL is a good cost function when the quantum data ensemble has a certain structure, i.e., it is confined in a relatively low dimensional manifold. In addition, We numerically showed that OTL can avoid the vanishing gradient issue thanks to the locality of the cost. Finally, we demonstrated the anomaly detection problems of quantum states, that cannot be handled via existing methods, to show a validity of our method.

There is still a lot of works to be done in the direction of this paper. First, this paper assumed that a quantum processing is performed individually for each quantum state, but it would be interesting to consider another setting such as allowing coherent access [1] or quantum memory [3]. In this scenario, the anomaly detection technique could be

used for processing quantum states which come from an external quantum processor, such as quantum sensor. Also, it would be interesting to extend the cost to the entropy regularized Wasserstein distance [56–60], which is effective for dealing with higher dimensional data in classical generative models. In this case, however, the localized cost proposed in this paper does not satisfy the axiom of distance likewise the case demonstrated in this paper; this is yet surely an interesting future work. Lastly, note that classical data can also be within the scope of our method, provided it can be effectively embedded into a quantum data; then the anomaly detection of financial data, which usually requires high dimensionality for precise detection, might be a suitable target.

Acknowledgement

This work was supported by MEXT Quantum Leap Flagship Program Grant Number JPMXS0118067285 and JP-MXS0120319794

References

- [1] Dorit Aharonov, Jordan Cotler, Xiao-Liang Qi. Quantum algorithmic measurement. *Nature Communications*, 13(1):1–9, 2022.
- [2] Yusen Wu, Bujiao Wu, Jingbo Wang, Xiao Yuan. Provable Advantage in Quantum Phase Learning via Quantum Kernel Alphasat. *arXiv preprint arXiv:2111.07553*, 2021.
- [3] Hsin-Yuan Huang *et al.* Quantum advantage in learning from experiments. *arXiv preprint arXiv:2112.00778*, 2021.
- [4] Jianmin Bao, Dong Chen, Fang Wen, Houqiang Li, Gang Hua. CVAE-GAN: fine-grained image generation through asymmetric training. In *Proceedings of the IEEE international conference on computer vision*, pages 2745–2754, 2017.
- [5] Andrew Brock, Jeff Donahue, Karen Simonyan. Large scale GAN training for high fidelity natural image synthesis. CoRR abs/1809.11096 (2018). *arXiv preprint arXiv:1809.11096*, 1809.
- [6] Tejas D Kulkarni, William F Whitney, Pushmeet Kohli, Josh Tenenbaum. Deep convolutional inverse graphics network. *Advances in neural information processing systems*, 28, 2015.
- [7] Rafael Gómez-Bombarelli, Jennifer N Wei, David Duvenaud, José Miguel Hernández-Lobato, Benjamín Sánchez-Lengeling, Dennis Sheberla, Jorge Aguilera-Iparraguirre, Timothy D Hirzel, Ryan P Adams, Alán Aspuru-Guzik. Automatic chemical design using a data-driven continuous representation of molecules. *ACS central science*, 4(2):268–276, 2018.
- [8] Chong Zhou, Randy C Paffenroth. Anomaly detection with robust deep autoencoders. In *Proceedings of the 23rd ACM SIGKDD international conference on knowledge discovery and data mining*, pages 665–674, 2017.
- [9] Marcello Benedetti, Delfina Garcia-Pintos, Oscar Perdomo, Vicente Leyton-Ortega, Yunseong Nam, Alejandro Perdomo-Ortiz. A generative modeling approach for benchmarking and training shallow quantum circuits. *npj Quantum Information*, 5(1):1–9, 2019.
- [10] Brian Coyle, Daniel Mills, Vincent Danos, Elham Kashefi. The Born supremacy: quantum advantage and training of an Ising Born machine. *npj Quantum Information*, 6(1):1–11, 2020.
- [11] Seth Lloyd, Christian Weedbrook. Quantum generative adversarial learning. *Physical review letters*, 121(4):040502, 2018.
- [12] Pierre-Luc Dallaire-Demers, Nathan Killoran. Quantum generative adversarial networks. *Physical Review A*, 98(1):012324, 2018.
- [13] Jonathan Romero, Jonathan P Olson, Alan Aspuru-Guzik. Quantum autoencoders for efficient compression of quantum data. *Quantum Science and Technology*, 2(4):045001, 2017.
- [14] Kwok Ho Wan, Oscar Dahlsten, Hlér Kristjánsson, Robert Gardner, MS Kim. Quantum generalisation of feed-forward neural networks. *npj Quantum information*, 3(1):1–8, 2017.
- [15] Li Zhou, Nengkun Yu, Shenggang Ying, Mingsheng Ying. Quantum earth mover’s distance, a no-go quantum kantorovich–rubinstein theorem, and quantum marginal problem. *Journal of Mathematical Physics*, 63(10):102201, 2022.
- [16] Giacomo De Palma, Milad Marvian, Dario Trevisan, Seth Lloyd. The quantum wasserstein distance of order 1. *IEEE Transactions on Information Theory*, 67(10):6627–6643, 2021.

- [17] Shouvanik Chakrabarti, Huang Yiming, Tongyang Li, Soheil Feizi, Xiaodi Wu. Quantum Wasserstein generative adversarial networks. In H. Wallach, H. Larochelle, A. Beygelzimer, F. d'Alché-Buc, E. Fox, R. Garnett, editors, *Advances in Neural Information Processing Systems*, volume 32. Curran Associates, Inc., 2019.
- [18] Bobak Toussi Kiani, Giacomo De Palma, Milad Marvian, Zi-Wen Liu, Seth Lloyd. Learning quantum data with the quantum earth mover's distance. *Quantum Science and Technology*, 7(4):045002, 2022.
- [19] Jarrod R McClean, Sergio Boixo, Vadim N Smelyanskiy, Ryan Babbush, Hartmut Neven. Barren plateaus in quantum neural network training landscapes. *Nature communications*, 9(1):1–6, 2018.
- [20] Leon Bottou, Martin Arjovsky, David Lopez-Paz, Maxime Oquab. Geometrical insights for implicit generative modeling. In *Braverman Readings in Machine Learning. Key Ideas from Inception to Current State*, pages 229–268. Springer, 2018.
- [21] Diederik P Kingma, Max Welling. Auto-encoding variational bayes. *arXiv preprint arXiv:1312.6114*, 2013.
- [22] Ian Goodfellow, Jean Pouget-Abadie, Mehdi Mirza, Bing Xu, David Warde-Farley, Sherjil Ozair, Aaron Courville, Yoshua Bengio. Generative adversarial nets. *Advances in neural information processing systems*, 27, 2014.
- [23] Danilo Rezende, Shakir Mohamed. Variational inference with normalizing flows. In *International conference on machine learning*, pages 1530–1538. PMLR, 2015.
- [24] Gabriel Peyre, Marco Cuturi. *Computational Optimal Transport: With Applications to Data Science (Foundations and Trends in Machine Learning)*. Now Publishers, paperback edition, 2 2019.
- [25] Yann Ollivier, Pajot Hervé, Cedric Villani, editors. *Optimal Transport: Theory and Applications*. London Mathematical Society Lecture Note Series. Cambridge University Press, 2014.
- [26] Filippo Santambrogio. Optimal transport for applied mathematicians. *Birkhäuser, NY*, 55(58-63):94, 2015.
- [27] Gabriel Peyre, Marco Cuturi. Editorial IMA IAI - Information and Inference special issue on optimal transport in data sciences. *Information and Inference: A Journal of the IMA*, 8(4):655–656, 12 2019.
- [28] Grégoire Montavon, Klaus-Robert Müller, Marco Cuturi. Wasserstein training of restricted Boltzmann machines. *Advances in Neural Information Processing Systems*, 29, 2016.
- [29] Espen Bernton, Pierre E Jacob, Mathieu Gerber, Christian P Robert. Inference in generative models using the Wasserstein distance. *arXiv preprint arXiv:1701.05146*, 1(8):9, 2017.
- [30] Martin Arjovsky, Soumith Chintala, Léon Bottou. Wasserstein generative adversarial networks. In *International conference on machine learning*, pages 214–223. PMLR, 2017.
- [31] Ilya Tolstikhin, Olivier Bousquet, Sylvain Gelly, Bernhard Schoelkopf. Wasserstein auto-encoders. *arXiv preprint arXiv:1711.01558*, 2017.
- [32] Aude Genevay, Gabriel Peyré, Marco Cuturi. GAN and VAE from an optimal transport point of view. *arXiv preprint arXiv:1706.01807*, 2017.
- [33] Olivier Bousquet, Sylvain Gelly, Ilya Tolstikhin, Carl-Johann Simon-Gabriel, Bernhard Schoelkopf. From optimal transport to generative modeling: the VEGAN cookbook. *arXiv preprint arXiv:1705.07642*, 2017.
- [34] Leonid V Kantorovich. On the translocation of masses. In *Dokl. Akad. Nauk. USSR (NS)*, volume 37, pages 199–201, 1942.
- [35] Cédric Villani. *Optimal transport: old and new*, volume 338. Springer, 2009.
- [36] Richard Mansfield Dudley. The speed of mean Glivenko-Cantelli convergence. *The Annals of Mathematical Statistics*, 40(1):40–50, 1969.
- [37] Jonathan Weed, Francis Bach. Sharp asymptotic and finite-sample rates of convergence of empirical measures in Wasserstein distance. *Bernoulli*, 25(4A):2620–2648, 2019.
- [38] Michael A. Nielsen, Isaac L. Chuang. *Quantum Computation and Quantum Information (Cambridge Series on Information and the Natural Sciences)*. Cambridge University Press, paperback edition, 9 2000.
- [39] Harry Buhrman, Richard Cleve, John Watrous, Ronald De Wolf. Quantum fingerprinting. *Physical Review Letters*, 87(16):167902, 2001.
- [40] Vojtěch Havlíček, Antonio D Córcoles, Kristan Temme, Aram W Harrow, Abhinav Kandala, Jerry M Chow, Jay M Gambetta. Supervised learning with quantum-enhanced feature spaces. *Nature*, 567(7747):209–212, 2019.

- [41] Kouhei Nakaji, Naoki Yamamoto. Expressibility of the alternating layered ansatz for quantum computation. *Quantum*, 5:434, 2021.
- [42] Marco Cerezo, Akira Sone, Tyler Volkoff, Lukasz Cincio, Patrick J Coles. Cost function dependent barren plateaus in shallow parametrized quantum circuits. *Nature communications*, 12(1):1–12, 2021.
- [43] Sumeet Khatri, Ryan LaRose, Alexander Poremba, Lukasz Cincio, Andrew T Sornborger, Patrick J Coles. Quantum-assisted quantum compiling. *Quantum*, 3:140, 2019.
- [44] Kunal Sharma, Sumeet Khatri, Marco Cerezo, Patrick J Coles. Noise resilience of variational quantum compiling. *New Journal of Physics*, 22(4):043006, 2020.
- [45] Alba Cervera-Lierta, Jakob S Kottmann, Alán Aspuru-Guzik. Meta-variational quantum eigensolver: Learning energy profiles of parameterized hamiltonians for quantum simulation. *PRX Quantum*, 2(2):020329, 2021.
- [46] Kosuke Mitarai, Makoto Negoro, Masahiro Kitagawa, Keisuke Fujii. Quantum circuit learning. *Physical Review A*, 98(3):032309, 2018.
- [47] Maria Schuld, Ville Bergholm, Christian Gogolin, Josh Izaac, Nathan Killoran. Evaluating analytic gradients on quantum hardware. *Physical Review A*, 99(3):032331, 2019.
- [48] MD SAJID ANIS *et al.* Qiskit: An Open-source Framework for Quantum Computing, 2021.
- [49] Zoë Holmes, Kunal Sharma, Marco Cerezo, Patrick J Coles. Connecting ansatz expressibility to gradient magnitudes and barren plateaus. *PRX Quantum*, 3(1):010313, 2022.
- [50] Varun Chandola, Arindam Banerjee, Vipin Kumar. Anomaly detection: A survey. *ACM computing surveys (CSUR)*, 41(3):1–58, 2009.
- [51] Satoshi Hara, Takafumi Ono, Ryo Okamoto, Takashi Washio, Shigeki Takeuchi. Anomaly detection in reconstructed quantum states using a machine-learning technique. *Physical Review A*, 89(2):022104, 2014.
- [52] Satoshi Hara, Takafumi Ono, Ryo Okamoto, Takashi Washio, Shigeki Takeuchi. Quantum-state anomaly detection for arbitrary errors using a machine-learning technique. *Physical Review A*, 94(4):042341, 2016.
- [53] T Ide. Introduction to Anomaly Detection Using Machine Learning—a Practical Guide With R (in Japanese). *Corona Publishing*, pages 132–139, 2015.
- [54] Thomas Schlegl, Philipp Seeböck, Sebastian M Waldstein, Ursula Schmidt-Erfurth, Georg Langs. Unsupervised anomaly detection with generative adversarial networks to guide marker discovery. In *International conference on information processing in medical imaging*, pages 146–157. Springer, 2017.
- [55] Diederik P Kingma, Jimmy Ba. Adam: A method for Stochastic Optimization. *arXiv:1412.6980*, December 2014.
- [56] Marco Cuturi. Sinkhorn distances: Lightspeed computation of optimal transport. *Advances in neural information processing systems*, 26:2292–2300, 2013.
- [57] Jean Feydy, Thibault Séjourné, François-Xavier Vialard, Shun-ichi Amari, Alain Trounev, Gabriel Peyré. Interpolating between Optimal Transport and MMD using Sinkhorn Divergences. arxiv e-prints, page. *arXiv preprint arXiv:1810.08278*, 2018.
- [58] Aude Genevay, Lénaïc Chizat, Francis Bach, Marco Cuturi, Gabriel Peyré. Sample complexity of Sinkhorn divergences. In *The 22nd International Conference on Artificial Intelligence and Statistics*, pages 1574–1583. PMLR, 2019.
- [59] Shun-ichi Amari, Naotsugu Tsuchiya, Masafumi Oizumi. Geometry of information integration. In *Information Geometry and its Applications IV*, pages 3–17. Springer, 2016.
- [60] Shun-ichi Amari, Ryo Karakida, Masafumi Oizumi. Information geometry connecting Wasserstein distance and Kullback–Leibler divergence via the entropy-relaxed transportation problem. *Information Geometry*, 1(1):13–37, 2018.
- [61] Laurens De Haan, Ana Ferreira, Ana Ferreira. *Extreme value theory: an introduction*, volume 21. Springer, 2006.

Appendices

A Proof of Proposition 9

Here, we give the proof of Proposition 9.

Proof. First, positivity $\mathcal{L}_c(\alpha, \beta) \geq 0$ is obvious from $c(\mathbf{x}, \mathbf{y}) \geq 0$ and $\pi(\mathbf{x}, \mathbf{y}) \geq 0$.

Next, we move on the proof of $\alpha = \beta \Rightarrow \mathcal{L}_c(\alpha, \beta) = 0$. When $\alpha = \beta$, then $\pi(\mathbf{x}, \mathbf{y}) = \alpha(\mathbf{x})\delta(\mathbf{x} - \mathbf{y})$ is one of the candidates that satisfy the constraint Eq. (2.3), which gives the following inequality:

$$\mathcal{L}_c(\alpha, \beta) \leq \int c(\mathbf{x}, \mathbf{y})\alpha(\mathbf{x})\delta(\mathbf{x} - \mathbf{y})d\mathbf{x}d\mathbf{y} = \int c(\mathbf{x}, \mathbf{x})\alpha(\mathbf{x})d\mathbf{x} = 0. \quad (\text{A.1})$$

Thus we obtain $\mathcal{L}_c(\alpha, \beta) = 0$.

Finally, we turn to $\mathcal{L}_c(\alpha, \beta) = 0 \Rightarrow \alpha = \beta$. When $\mathbf{x} \neq \mathbf{y}$, the ground distance $c(\mathbf{x}, \mathbf{y})$ is always greater than 0, and if the transport plan $\pi(\mathbf{x}, \mathbf{y})$ takes a nonzero value, then $\mathcal{L}_c(\alpha, \beta)$ is always greater than 0. This indicates that in order for $\mathcal{L}_c(\alpha, \beta) = 0$, the transport plan $\pi(\mathbf{x}, \mathbf{y})$ should be a function that concentrated on $\mathbf{x} = \mathbf{y}$, i.e., the transport plans can be written as $\pi(\mathbf{x}, \mathbf{y}) = f(\mathbf{x})\delta(\mathbf{x} - \mathbf{y})$ with Dirac delta function $\delta(\mathbf{x} - \mathbf{y})$. Then, the constraint $\int \pi(\mathbf{x}, \mathbf{y})d\mathbf{x} = \beta(\mathbf{x})$ of Eq. (2.3) leads to $f(\mathbf{y}) = \beta(\mathbf{y})$. Thus, we have $\pi(\mathbf{x}, \mathbf{y}) = \beta(\mathbf{x})\delta(\mathbf{x} - \mathbf{y})$, and we finally obtain $\alpha(\mathbf{x}) = \beta(\mathbf{x})$ by taking into account the constraint $\int \pi(\mathbf{x}, \mathbf{y})d\mathbf{y} = \alpha(\mathbf{x})$. \square

B Simulation results of Eq.(4.7)

Here, we give the result of numerical simulations for the approximate error of the empirical loss Eq. (4.6) and the result of fitting them with Eq. (4.7). The results are shown in Fig.10. The parameters of the simulation are given in Table 1. Fig.3 are created based on the result of Fig.10.

C Proof of Proposition 12

Here, we provide the proof of Proposition 12 in Sec. 4.2. To prove the proposition, we exploit the following lemma.

Lemma 13. *Suppose that X_i ($i = 1, 2, \dots, N_s$) are i.i.d. random variables with positive values and expected value $p = \mathbb{E}[X_i]$. Then, the following inequalities hold for the expected value of root mean $\mathbb{E}[\sqrt{\bar{X}}]$ and the variance $\mathbb{V}[\sqrt{\bar{X}}]$ of $\bar{X} = \frac{1}{N_s} \sum_{i=1}^{N_s} X_i$:*

$$\sqrt{p} - \frac{1-p}{2N_s\sqrt{p}} \leq \mathbb{E}[\sqrt{\bar{X}}] \leq \sqrt{p}, \quad (\text{C.1})$$

$$\mathbb{V}[\sqrt{\bar{X}}] \leq \frac{1-p}{N_s} + \frac{(1-p)^2}{4N_s^2p}. \quad (\text{C.2})$$

Proof. The inequality on the right side of Eq. (C.1) is obvious from Jensen's inequality. The inequality on the left side of Eq. (C.1) can be obtained by substituting $r = \frac{\bar{X}}{\mathbb{E}(\bar{X})}$ into the the inequality $\sqrt{r} \geq \frac{-r^2+3r}{2}$, which holds for any non-negative number r . The second inequality for the variance Eq. (C.2) be obtained by substituting the first inequality Eq. (C.1) into the definition of the variance $\mathbb{V}[\sqrt{\bar{X}}] = \mathbb{E} \left[\left(\sqrt{\bar{X}} - \mathbb{E}(\sqrt{\bar{X}}) \right)^2 \right]$. \square

Here, the random variable of this lemma X_i would be identified with the random variable $X_i = \sum_{k=1}^n X_{i,j,k}^{(s)}$, where $X_{i,j,k}^{(s)}$ is defined just above Eq. (3.8).

Next, we consider the following lemma, which indicates that if the difference between two ground costs c_1, c_2 is sufficiently small, the difference between corresponding two optimal transport losses $\mathcal{L}_{c^1}, \mathcal{L}_{c^2}$ is also sufficiently small.

Lemma 14. *Denote the optimal transport plans of Eq. (2.3) between the empirical distributions $\hat{\alpha}_M(x) = \frac{1}{M} \sum_{i=1}^M \delta(\mathbf{x} - \mathbf{x}_i)$ and $\hat{\beta}_M(y) = \frac{1}{M} \sum_{j=1}^M \delta(\mathbf{y} - \mathbf{y}_j)$ for two different ground costs c_1 and c_2 as $\pi_{i,j}^1 = \pi^1(\mathbf{x}_i, \mathbf{y}_j)$ and $\pi_{i,j}^2 = \pi^2(\mathbf{x}_i, \mathbf{y}_j)$, respectively. Also, denote the non-zero components of the optimal transport plans $\pi_{i,j}^1$ and $\pi_{i,j}^2$ as $A^1 = \{(i, j) | \pi_{i,j}^1 > 0\}$ and $A^2 = \{(i, j) | \pi_{i,j}^2 > 0\}$, respectively. Suppose that the difference between the ground costs c_1 and c_2 for any $(i, j) \in A^1 \cup A^2$ is upper bounded with a constant t as follows:*

$$|c^1(\mathbf{x}_i, \mathbf{y}_j) - c^2(\mathbf{x}_i, \mathbf{y}_j)| < t. \quad (\text{C.3})$$

Then, the difference between the corresponding optimal transport losses \mathcal{L}_{c^1} and \mathcal{L}_{c^2} follows

$$|\mathcal{L}_{c^1}(\hat{\alpha}_M, \hat{\beta}_M) - \mathcal{L}_{c^2}(\hat{\alpha}_M, \hat{\beta}_M)| < t. \quad (\text{C.4})$$

Proof. Here, we only show the proof of $\mathcal{L}_{c^1}(\hat{\alpha}_M, \hat{\beta}_M) - \mathcal{L}_{c^2}(\hat{\alpha}_M, \hat{\beta}_M) < t$. The other inequality $\mathcal{L}_{c^2}(\hat{\alpha}_M, \hat{\beta}_M) - \mathcal{L}_{c^1}(\hat{\alpha}_M, \hat{\beta}_M) < t$ can be proved in the same way.

$$\begin{aligned}
\mathcal{L}_{c^1}(\hat{\alpha}_M, \hat{\beta}_M) - \mathcal{L}_{c^2}(\hat{\alpha}_M, \hat{\beta}_M) &= \min_{\pi} \int c^1(\mathbf{x}, \mathbf{y}) d\pi(\mathbf{x}, \mathbf{y}) - \min_{\pi} \int c^2(\mathbf{x}, \mathbf{y}) d\pi(\mathbf{x}, \mathbf{y}) \\
&= \min_{\pi} \int c^1(\mathbf{x}, \mathbf{y}) d\pi(\mathbf{x}, \mathbf{y}) - \sum_{i,j=1}^M c^2(\mathbf{x}_i, \mathbf{y}_j) \pi^2(\mathbf{x}_i, \mathbf{y}_j) \\
&\leq \sum_{i,j=1}^M c^1(\mathbf{x}_i, \mathbf{y}_j) \pi^2(\mathbf{x}_i, \mathbf{y}_j) - \sum_{i,j=1}^M c^2(\mathbf{x}_i, \mathbf{y}_j) \pi^2(\mathbf{x}_i, \mathbf{y}_j) \\
&\leq \sum_{i,j=1}^M t \pi^2(\mathbf{x}_i, \mathbf{y}_j) = t
\end{aligned}$$

□

Lemma 14 immediately leads the following lemma.

Lemma 15. *Given a set of positive constant t and δ , which satisfies*

$$P(|c^1(\mathbf{x}_i, \mathbf{y}_j) - c^2(\mathbf{x}_i, \mathbf{y}_j)| \geq t) \leq \frac{\delta}{2M} \quad (\text{C.5})$$

for any component $i, j \in \{1, 2, \dots, M\}$, where the notations are same as Lemma 14. Then, the following inequality holds for the corresponding optimal transport losses:

$$P(|\mathcal{L}_{c^1}(\hat{\alpha}_M, \hat{\beta}_M) - \mathcal{L}_{c^2}(\hat{\alpha}_M, \hat{\beta}_M)| \geq t) \leq \delta. \quad (\text{C.6})$$

Proof. For simplicity, we prove only for the the solution of the optimal transport plan that M components take the value $1/M$ and the other components take the value 0, but proofs for the other solutions can be performed in the same manner. For such a solution, the number of non-zero components is at most $|A^1 \cup A^2| \leq 2M$, and using the assumption Eq. (C.5), the probability that those non-zero components have an error within t is upper bounded as

$$P\left(\bigcap_{(i,j) \in A^1 \cup A^2} |c^1(\mathbf{x}_i, \mathbf{y}_j) - c^2(\mathbf{x}_i, \mathbf{y}_j)| < t\right) > \left(1 - \frac{\delta}{2M}\right)^{2M} \geq 1 - \delta. \quad (\text{C.7})$$

Then, Lemma 15 can be straightforwardly proven by taking into account that Lemma 14 leads

$$P\left(\bigcap_{(i,j) \in A^1 \cup A^2} |c^1(\mathbf{x}_i, \mathbf{y}_j) - c^2(\mathbf{x}_i, \mathbf{y}_j)| < t\right) \leq P(|\mathcal{L}_{c^1}(\hat{\alpha}_M, \hat{\beta}_M) - \mathcal{L}_{c^2}(\hat{\alpha}_M, \hat{\beta}_M)| \leq t). \quad (\text{C.8})$$

□

Now, we are ready to prove Proposition 12.

Proof. Under the same setting as Lemma 13, Chebyshev inequality for the random variable \sqrt{X} leads, with some positive constant k ,

$$\begin{aligned}
\frac{1}{k^2} &\geq P\left(\left|\sqrt{X} - \mathbb{E}(\sqrt{X})\right| \geq k\sqrt{\mathbb{V}[\sqrt{X}]}\right) \\
&\geq P\left(\left|\sqrt{X} - \sqrt{p}\right| - \left|\sqrt{p} - \mathbb{E}(\sqrt{X})\right| \geq k\sqrt{\mathbb{V}[\sqrt{X}]}\right) \\
&\geq P\left(\left|\sqrt{X} - \sqrt{p}\right| \geq k\sqrt{\frac{1-p}{N_s} + \frac{(1-p)^2}{4N_s^2 p} + \frac{1-p}{2N_s\sqrt{p}}}\right)
\end{aligned} \quad (\text{C.9})$$

By setting $\sqrt{X} = \mathcal{L}_{\tilde{c}}$ and $\sqrt{p} = \mathcal{L}_c$, and comparing Eqs.(C.5) and (C.9), we obtain Proposition 12 by setting

$$t = \sqrt{\frac{2n}{\delta}} \sqrt{\frac{1-p}{N_s} + \frac{(1-p)^2}{4N_s^2 p} + \frac{1-p}{2N_s\sqrt{p}}}.$$

□

D Intuitive explanation on the shape of Fig.4

Here, we give the rough explanation of the dependence of the mean approximation error on the number of training data, presented in Fig.10 of Sec.4.2. Throughout this section, we assume that the number of shots N_s is sufficiently large to hold the asymptotic theory.

We first focus on the case of small number of training data M , where the approximation error behaves like $M^{-1/2}$. In this case, the training data $\{\mathbf{x}_i\}_{i=1}^M$ would be well separated from each other and the optimal transport plan $\{\pi_{i,j}\}_{i,j=1}^M$ is not expected to be affected by the number of shots N_s . In most cases, the number of non-zero elements of optimal transport plan $A = \{(i,j)|\pi_{i,j} > 0\}$ is M and the value of those are $1/M$.

The estimated value of the ground cost $c_{\text{local},i,j}$ of Eq. (3.8) with N_s shots is given by $\tilde{c}_{\text{local},i,j}^{(N_s)} = \sqrt{\frac{1}{n} \sum_{k=1}^n \frac{1}{N_s} \sum_{s=1}^{N_s} X_{i,j,k}^{(s)}}$, where $X_{i,j,k}^{(s)}$ are random variables following the Bernoulli distribution with probability $1 - p_{i,j}^{(k)}$. Due to the central limit theorem, the inside of the root $Y_{i,j}^{(s)} = \frac{1}{n} \sum_{k=1}^n X_{i,j,k}^{(s)}$ asymptotically converge to a normal distribution $\sqrt{N_s}(\sum_{s=1}^{N_s} Y_{i,j}^{(s)}/N_s - \mu_{i,j}) \sim \mathcal{N}(0, \sigma_{i,j}^2)$ with mean $\mu_{i,j} = \sum_{k=1}^n (1 - p_{i,j}^{(k)})$ and variance $\sigma_{i,j}^2 = \sum_{k=1}^n (1 - p_{i,j}^{(k)})p_{i,j}^{(k)}$. Thus, delta method tells us that the approximation error of the ground cost follows $\sqrt{N_s}(\tilde{c}_{\text{local},i,j}^{(N_s)} - c_{\text{local},i,j}) \sim \mathcal{N}(0, \frac{\sigma_{i,j}^2}{4\mu_{i,j}})$.

Assume that the means and variances are almost the same for all the components, i.e., $\mu_{i,j} \approx \mu$, $\sigma_{i,j} \approx \sigma \forall i,j$, the approximation error of the optimal transport loss due to the number of shots can be written as

$$\begin{aligned} \mathcal{L}_{\tilde{c}_{\text{local}}^{(N_s)}} - \mathcal{L}_{c_{\text{local}}} &= \frac{1}{M} \sum_{(i,j) \in A} \left(\tilde{c}_{\text{local},i,j}^{(N_s)} - c_{\text{local},i,j} \right) \\ &\sim \mathcal{N} \left(0, \sum_{(i,j) \in A} \frac{\sigma_{i,j}^2}{4N_s \mu_{i,j} M^2} \right) \\ &\approx \mathcal{N} \left(0, \frac{\sigma^2}{4N_s \mu M} \right). \end{aligned} \quad (\text{D.1})$$

Thus the approximation error with small number of training data behaves like $(N_s M)^{-1/2}$ under the condition shown here.

On the other hand, behavior of the approximation error in the range of large number of training data M is explained by the theory of the extreme value distribution [61]. In the case of large number of training data, it would be expected that there are many ground costs $c_{\text{local},i,j}$ with almost the same value. As an extreme case, consider the case where all ground costs have a common constant value, $c_{\text{local},i,j} = c$, $\forall i,j$. Again assume that the number of shots N_s is sufficiently large, then the ground cost $\tilde{c}_{\text{local},i,j}^{(N_s)}$ follows a normal distribution, which we denote as $\mathcal{N}(c, \frac{\sigma^2}{N_s})$. Then, using i.i.d random numbers $\{X_{i,j}\}_{i,j=1}^M$ which follow a normal distribution $\mathcal{N}(0, \frac{\sigma^2}{N_s})$, the approximation error can be written as

$$\begin{aligned} \mathcal{L}_{\tilde{c}_{\text{local}}^{(N_s)}} - \mathcal{L}_{c_{\text{local}}} &\approx \min_{\{\pi_{i,j}\}_{i,j=1}^M} \sum_{i,j=1}^M X_{i,j} \pi_{i,j}, \\ \text{subject to } \sum_{i=1}^M \pi_{i,j} &= \frac{1}{M}, \sum_{j=1}^{M_g} \pi_{i,j} = \frac{1}{M}, \pi_{i,j} \geq 0. \end{aligned} \quad (\text{D.2})$$

Now we approximate this minimization by greedy algorithm, i.e., consider first obtaining the minimum value X_{i_1, j_1} from the M^2 components, and then the second minimum value X_{i_2, j_2} from the rest $(M-1)^2$ components other than i -th row and j -th column, and so on. Denoting the cumulative distribution function of a random variable $X_{i,j}$ as $F(x)$, the distribution of the minimum value of the k data can be written as

$$\begin{aligned} G(x, k) &= 1 - (1 - F(x))^k, \\ p(x, k) &= \frac{dG(x, k)}{dx} = k \frac{dF(x)}{dx} (1 - F(x))^{k-1}. \end{aligned} \quad (\text{D.3})$$

Then the probability density at which $x_1, x_2, x_3, \dots, x_M$ are obtained from the greedy algorithm is given as

$$\begin{aligned} &p(x_1, x_2, \dots, x_M) \\ &= p(x_1, M^2) \frac{p(x_2, (M-1)^2) \theta(x_2 - x_1)}{1 - G(x_1, (M-1)^2)} \frac{p(x_3, (M-2)^2) \theta(x_3 - x_2)}{1 - G(x_2, (M-2)^2)} \times \dots \times \frac{p(x_M, 1^2) \theta(x_M - x_{M-1})}{1 - G(x_{M-1}, 1^2)} \\ &= \prod_{k=1}^M \frac{k^2}{2k-1} p(x_k, 2k-1) \theta(x_k - x_{k-1}), \end{aligned} \quad (\text{D.4})$$

where $\theta(x)$ denotes a step function, and we set $x_0 = -\infty$ in the last expression. Finally, we approximate this expression by the mode. Then, from the theory of the extreme value distribution, the mode of $p(x, k)$ can be written

as $x_{mode} \approx -\sigma\sqrt{2\ln M/N_s}$ and we reach

$$\begin{aligned}\mathcal{L}_{c_{\text{local}}^{(N_s)}} - \mathcal{L}_{c_{\text{local}}} &\approx \frac{\sigma}{\sqrt{N_s}} \left(\frac{1}{M} \sum_{k=1}^M \sqrt{2\ln(2k-1)} \right) \\ &\approx \frac{\sigma}{\sqrt{N_s}} \sqrt{2\ln(2M-1)}.\end{aligned}\tag{D.5}$$

Thus we can roughly understand that the approximation error with large number of training data behaves like $N_s^{-1/2}\sqrt{\ln(M)}$.

E Simulation results of Sec.4.3

Here, we give the numerical simulation results on the variance in the gradient of the proposed cost function. As discussed in Sec.4.3, we introduce the loss function with the ground cost calculated by the local cost defined in Eq. (3.3), and it avoids the vanishing of the gradient. The results based on different data numbers are shown in Fig.11. The parameters of the simulation are given in Table 3. Fig.5(c) is created based on the result of Fig.11.

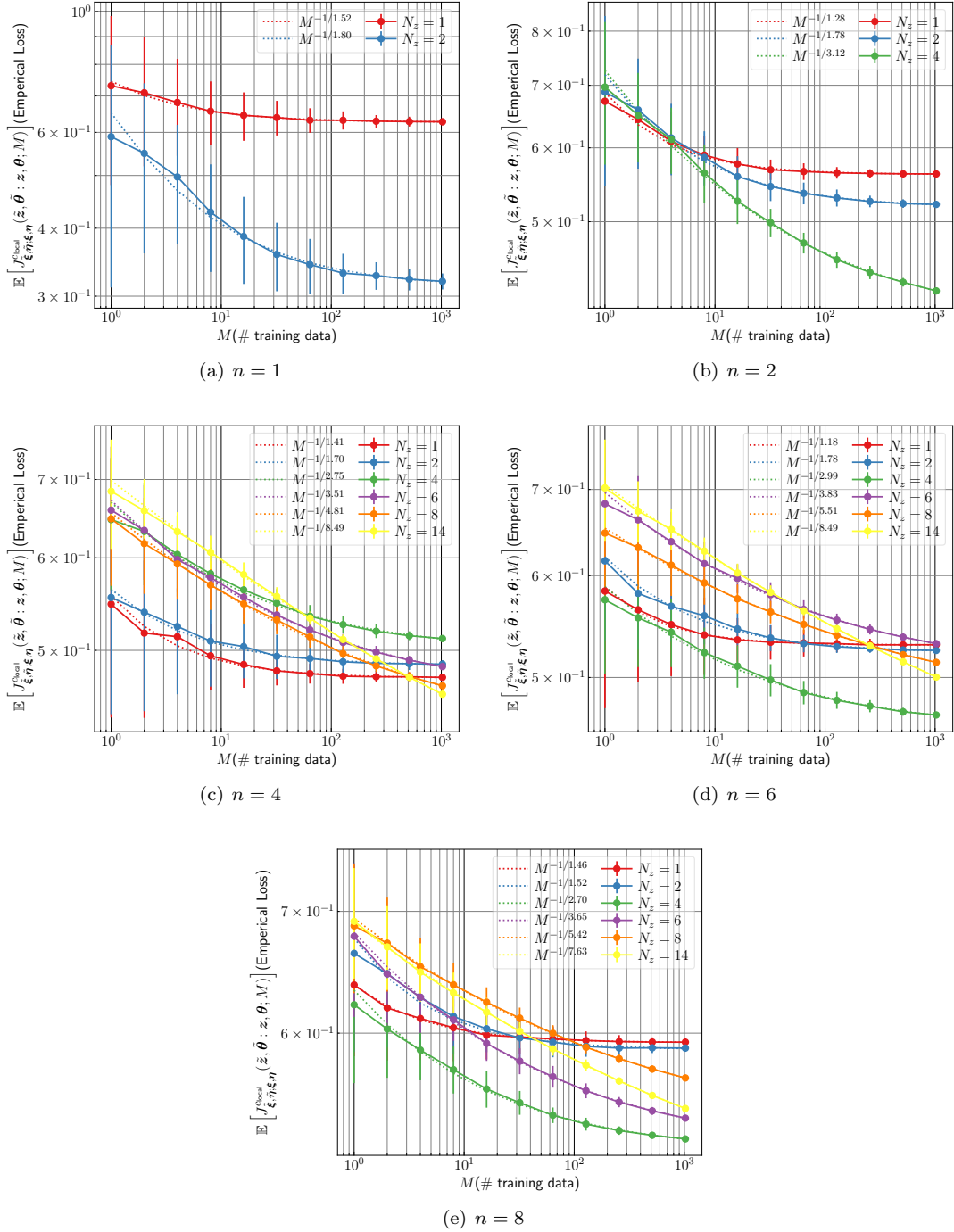
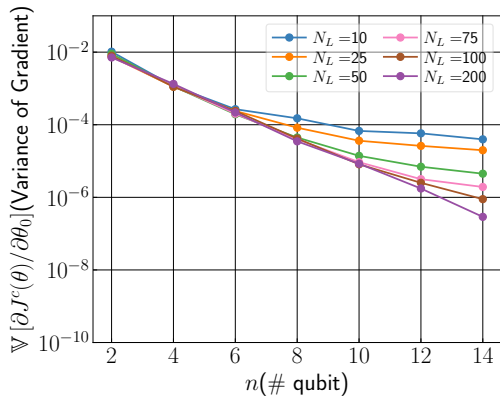
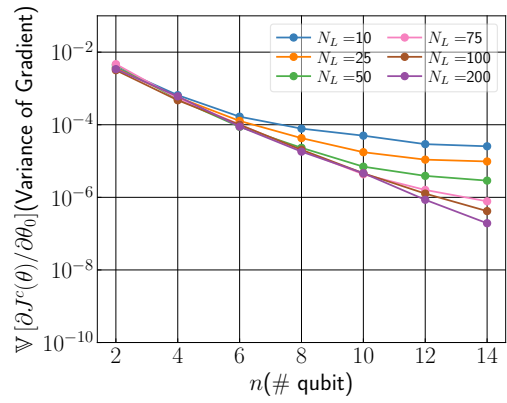


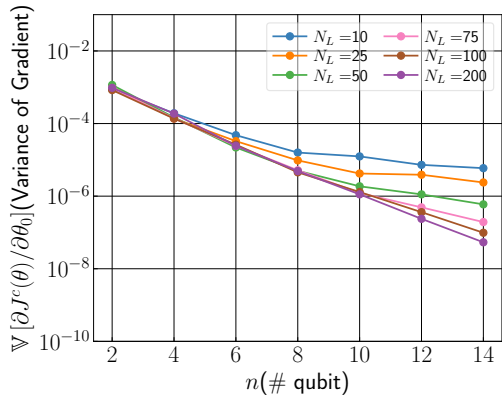
Figure 10: Simulation results of relationship between the approximation error of the proposed loss Eq. (4.6) and number of training data M . These points represent the result of the proposed loss, and the dotted lines represent the fitting result with Eq. (4.7). The values of parameter B obtained by the fitting is shown in the legend of the dotted lines.



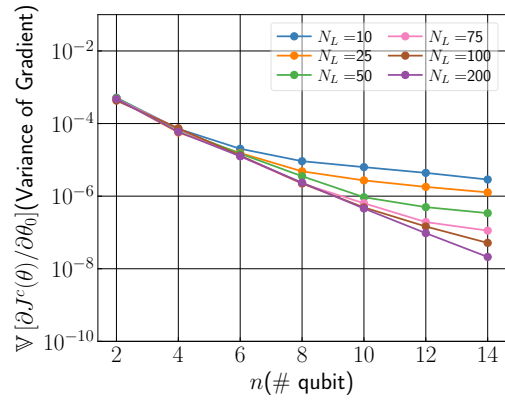
(a) $M = 1$



(b) $M = 2$



(c) $M = 8$



(d) $M = 16$

Figure 11: Simulation results of relationship between the number of qubit and the variance of the gradient of the proposed loss, which is based on local cost.